CENTRAL RESEARCH LIBRARY
DOCUMENT COLLECTION

[redacted]

ORNL-2274, Part 6 cy. 127-A
C-85 – Reactors-Aircraft Nuclear Propulsion Systems

AEC RESEARCH AND DEVELOPMENT REPORT

MARTIN MARIETTA ENERGY SYSTEMS LIBRARIES
3 4456 0251031 6

DECLASSIFIED
CLASSIFICATION CHANGED TO:
BY AUTHORITY OF: AEC 6-25-66
BY: E. Ackermann 2-14-67

AIRCRAFT NUCLEAR PROPULSION PROJECT

QUARTERLY PROGRESS REPORT

FOR PERIOD ENDING MARCH 31, 1957

CENTRAL RESEARCH LIBRARY
DOCUMENT COLLECTION
LIBRARY LOAN COPY
DO NOT TRANSFER TO ANOTHER PERSON
If you wish someone else to see this document, send in name with document and the library will arrange a loan.

[redacted]

OAK RIDGE NATIONAL LABORATORY
OPERATED BY
UNION CARBIDE NUCLEAR COMPANY
A Division of Union Carbide and Carbon Corporation
UCC
POST OFFICE BOX X · OAK RIDGE, TENNESSEE

[redacted]

This document contains Restricted Data as defined in the Atomic Energy Act of 1954. Its transmission or the disclosure of its contents in any manner to an unauthorized person is prohibited.

[redacted]

LEGAL NOTICE

This report was prepared as an account of Government sponsored work. Neither the United States, nor the Commission, nor any person acting on behalf of the Commission:

A. Makes any warranty or representation, express or implied, with respect to the accuracy, completeness, or usefulness of the information contained in this report, or that the use of any information, apparatus, method, or process disclosed in this report may not infringe privately owned rights; or

B. Assumes any liabilities with respect to the use of, or for damages resulting from the use of any information, apparatus, method, or process disclosed in this report.

As used in the above, "person acting on behalf of the Commission" includes any employee or contractor of the Commission to the extent that such employee or contractor prepares, handles or distributes, or provides access to, any information pursuant to his employment or contract with the Commission.

[redacted]

ORNL-2274, Part 6
C-85 – Reactors-Aircraft Nuclear Propulsion Systems

This document consists of 52 pages.

Copy 127 of 226 copies. Series A.

Contract No. W-7405-eng-26

AIRCRAFT NUCLEAR PROPULSION PROJECT

QUARTERLY PROGRESS REPORT

For Period Ending March 31, 1957

W. H. Jordan, Director
S. J. Cromer, Co-Director
A. J. Miller, Assistant Director

DATE ISSUED

JUL 22 1957

OAK RIDGE NATIONAL LABORATORY
Operated by
UNION CARBIDE NUCLEAR COMPANY
A Division of Union Carbide and Carbon Corporation
Post Office Box X
Oak Ridge, Tennessee

[redacted]

MARTIN MARIETTA ENERGY SYSTEMS LIBRARIES

3 4456 0251031 6

[redacted]

ORNL-2274, Part 6
C-[redacted] – Reactors-Aircraft Nuclear Propulsion Systems

INTERNAL DISTRIBUTION

1. R. G. Affel
2. C. J. Barton
3. M. Bender
4. D. S. Billington
5. F. F. Blankenship
6. E. P. Blizard
7. C. J. Borkowski
8. W. F. Boudreau
9. G. E. Boyd
10. M. A. Bredig
11. E. J. Breeding
12. W. E. Browning
13. F. R. Bruce
14. A. D. Callihan
15. D. W. Cardwell
16. C. E. Center (K-25)
17. R. A. Charpie
18. R. L. Clark
19. C. E. Clifford
20. J. H. Coobs
21. W. B. Cottrell
22. D. D. Cowen
23. S. Cromer
24. R. S. Crouse
25. F. L. Culler
26. D. R. Cuneo
27. J. H. DeVan
28. L. M. Doney
29. D. A. Douglas
30. E. R. Dytko
31. W. K. Eister
32. L. B. Emlet (K-25)
33. D. E. Ferguson
34. A. P. Fraas
35. J. H. Frye
36. W. T. Furgerson
37. R. J. Gray
38. A. T. Gresky
39. W. R. Grimes
40. A. G. Grindell
41. E. Guth
42. C. S. Harrill
43. E. E. Hoffman
44. H. W. Hoffman
45. A. Hollaender
46. A. S. Householder
47. J. T. Howe
48. W. H. Jordan
49. G. W. Keilholtz
50. C. P. Keim
51. F. L. Keller
52. M. T. Kelley
53. F. Kertesz
54. J. J. Keyes
55. E. M. King
56-57. J. A. Lane
58. R. B. Lindauer
59. R. S. Livingston
60. R. N. Lyon
61. H. G. MacPherson
62. R. E. MacPherson
63. F. C. Maienschein
64. W. D. Manly
65. E. R. Mann
66. L. A. Mann
67. W. B. McDonald
68. J. R. McNally
69. F. R. McQuilkin
70. R. V. Meghreblian
71. R. P. Milford
72. A. J. Miller
73. R. E. Moore
74. J. G. Morgan
75. K. Z. Morgan
76. E. J. Murphy
77. J. P. Murray (Y-12)
78. M. L. Nelson
79. G. J. Nessle
80. R. B. Oliver
81. L. G. Overholser
82. P. Patriarca
83. S. K. Penny
84. A. M. Perry
85. J. C. Pigg
86. P. M. Reyling
87. A. E. Richt
88. M. T. Robinson
89. H. W. Savage
90. A. W. Savolainen
91. R. D. Schultheiss
92. D. Scott
93. J. L. Scott

[redacted]

[redacted]

94. E. D. Shipley
95. A. Simon
96. O. Sisman
97. J. Sites
98. M. J. Skinner
99. A. H. Snell
100. C. D. Susano
101. J. A. Swartout
102. E. H. Taylor
103. R. E. Thoma
104. D. B. Trauger
105. D. K. Trubey
106. G. M. Watson
107. A. M. Weinberg
108. J. C. White
109. G. D. Whitman
110. E. P. Wigner (consultant)
111. G. C. Williams
112. J. A. Wilson
113. C. E. Winters
114. E. Zobel
115-117. ORNL – Y-12 Technical Library Document Reference Section
118-124. Laboratory Records Department
125. Laboratory Records, ORNL R. C.
126-128. Central Research Library

EXTERNAL DISTRIBUTION

129. AF Plant Representative, Baltimore
130. AF Plant Representative, Burbank
131. AF Plant Representative, Clifton
132. AF Plant Representative, Long Beach
133-134. AF Plant Representative, Marietta
135-137. AF Plant Representative, Santa Monica
138-139. AF Plant Representative, Seattle
140. AF Plant Representative, Wichita
141. Air Research and Development Command (RDGN)
142. Air Technical Intelligence Center
143. Air University Library
144-146. ANP Project Office, Fort Worth
147. Argonne National Laboratory
148. Armed Forces Special Weapons Project, Sandia
149. Armed Forces Special Weapons Project, Washington
150. Assistant AF Plant Representative, Downey
151. Assistant Secretary of the Air Force, R&D
152-158. Atomic Energy Commission, Washington
159. Bureau of Aeronautics
160. Bureau of Aeronautics General Representative
161. Chicago Operations Office
162. Chicago Patent Group
163. Chief of Naval Research
164. Convair-General Dynamics Corporation
165. Curtiss-Wright Corporation
166-168. General Electric Company (ANPD)
169. Hartford Area Office
170. Headquarters, Air Force Special Weapons Center
171. Idaho Operations Office
172. Lockland Area Office
173. Los Alamos Scientific Laboratory
174. Marquardt Aircraft Company

[redacted]

[redacted]

175. National Advisory Committee for Aeronautics, Cleveland
176. National Advisory Committee for Aeronautics, Washington
177-179. Naval Air Development and Material Center
180. Naval Research Laboratory
181. North American Aviation, Inc. (Missile Development Division)
182. Nuclear Development Corporation of America
183. Office of Chief of Naval Operations (OP-361)
184. Patent Branch, Washington
185. Patterson-Moos
186-189. Pratt & Whitney Aircraft Division (Fox Project)
190. San Francisco Operations Office
191. Sandia Corporation
192. Sandia Corporation, Livermore
193. School of Aviation Medicine
194. USAF Headquarters
195. USAF Project RAND
196. U. S. Naval Radiological Defense Laboratory
197. University of California Radiation Laboratory, Livermore
198-215. Wright Air Development Center (WCOSI-3)
216-225. Technical Information Service Extension, Oak Ridge
226. Division of Research and Development AEC, ORO

[redacted]

FOREWORD

This portion, Part 6. Advanced Power Plant Design and Aircraft Shielding, of the Aircraft Nuclear Propulsion Project Quarterly Progress Report falls in AEC category C-85, Reactors – Aircraft Nuclear Propulsion Systems, and is therefore being issued separately in order not to further limit distribution of the material that falls in AEC category C-84, Reactors – Special Features of Aircraft Reactors, which has been issued as ORNL-2274, Parts 1–5.

[redacted]

CONTENTS

FOREWORD v

SUMMARY 1

PART 6. ADVANCED POWER PLANT DESIGN AND AIRCRAFT SHIELDING

6.1. ADVANCED POWER PLANT DESIGN 5

A Nuclear-Powered Transport Type of Aircraft with Turboprop Engines 5

Airframe 5

Engines 6

Reactor and Reactor Shield 9

Crew Shield 9

Chemical Auxiliary Engines 10

Weight and Payload Estimates 10

6.2. TOWER SHIELDING FACILITY 11

Irradiation of a Pratt & Whitney Aircraft J-57 Engine 11

Experimental Arrangement During the Irradiation 11

Gamma-Ray and Neutron Dose-Rate Measurements Preceding and During the Engine Exposure (Phases I and II) 11

Gamma-Ray Dose-Rate Measurements After Engine Exposure (Phase III) 12

Gamma-Ray Spectra Measurements After Engine Exposure (Phase III) 15

Analysis of Results 19

6.3. BULK SHIELDING FACILITY 21

Preliminary Measurement of the Spectrum of Prompt Gamma Rays from Thermal Fission of U^{235} 21

Experimental Apparatus 21

Preliminary Instrument Tests 21

Future Work 23

Analysis of the Fission-Product Gamma-Ray Energy Spectrum Experiment 23

After-Shutdown Gamma-Ray Dose Measurements 23

Feasibility Study of a Circulating-Fuel Reactor for Shielding Tests 25

Program for Shielding Measurements at the ART 25

Total Absorption Gamma-Ray Spectrometer 25

The BSF Model IV Gamma-Ray Spectrometer Housing and Positioner 27

A Low-Sensitivity Gamma-Ray Ion Chamber for Radiation Damage Studies 31

Pulsed-Neutron Method for the Determination of Neutron Diffusion Parameters in Beryllium 33

[redacted]

[redacted]

A UO_2–Stainless Steel Shield Test Reactor for the BSF 34
Description of the Reactor 34
Heat Transfer Calculations 37
Reactivity Calculations 38
Control Plate Experiments 41

[redacted]

[redacted]

ANP PROJECT QUARTERLY PROGRESS REPORT

SUMMARY

6.1. Advanced Power Plant

The results of a preliminary investigation indicate that the presently flying Douglas C-133A aircraft could be adapted for all-nuclear-powered flight with the use of a reflector-moderated circulating-fuel reactor of the ART type in conjunction with turboprop engines. The gross weight of such an aircraft, exclusive of payload but with shielding sufficient to limit the maximum crew-compartment dose rate to 0.02 rem/hr, would be approximately 230,000 lb. The payload would be 25,000 to 50,000 lb and would thus duplicate that of the present chemical-powered C-133A aircraft. The power of the reactor required for this application would be about 75 Mw. Such an all-nuclear-powered aircraft would be suitable for a wide variety of applications, including logistics transport, early-warning radar missions, and missile launching.

6.2. Tower Shielding Facility

A test of the compatibility of a jet engine and a reactor system was made with a Pratt & Whitney Aircraft J-57 model jet engine being operated continuously for 50 hr while it was exposed to a total tissue dose of 7×10^8 ergs/g from the Tower Shielding Facility reactor. The objectives of the experiment were to study effects of radiation on the control and performance of the engine, the radiation damage to engine components, and the induced radioactivation of the engine. Gamma-ray spectra and dose-rate measurements were taken immediately after exposure and for several days following exposure in an attempt to identify the elements which were emitting induced radioactivity. The analysis has thus far resulted in the identification of 2.76- and 1.38-Mev Na^{24} and 2.06-, 1.7-, and 0.83-Mev Mn^{56} gamma rays. A more detailed analysis is in progress. No deleterious effects on the performance of the engine were observed during the irradiation, and it has been returned to Pratt & Whitney Aircraft for radiation damage studies.

6.3. Bulk Shielding Facility

Equipment has been developed to experimentally measure the prompt-gamma-ray spectrum resulting from the thermal fission of U^{235}, in order that an accurate prompt-gamma-ray source term will be available for use in future calculations of the performance of reactor shields. The equipment consists of a spiral fission chamber viewed by the collimator of a multiple-crystal scintillation spectrometer. Gamma rays detected in the spectrometer are recorded if they are observed in time coincidence with the event in the fission chamber, within the experimental time resolution. This resolution has been narrowed to about 0.06 μsec. Preliminary instrument tests have been performed, and it is felt that only the linearity of the pulse analyzer must be improved before a satisfactory experiment can be performed.

In the continued analysis of the fission-product gamma-ray spectrum experiment, efforts have been concentrated on correcting the data for the nonuniqueness of the scintillation spectrometers. A method designed to remove almost completely the nonuniqueness effect failed in that the final results appear to be meaningless. It is not yet clear whether this failure was due to a mistake in execution or to the propagation of experimental error.

A preliminary experiment was performed to determine the after-shutdown gamma-ray dose emitted by the Bulk Shielding Facility reactor. In two independent tests, 24 hr apart, the reactor, which was loaded with fuel elements that contained fission products from previous operations, was operated at 100 kw for 1 hr and gamma-ray dose-rate measurements were taken for approximately 14 hr after shutdown. The results are presented.

A study was carried out to determine the feasibility of constructing a circulating-fuel reactor at the BSF for aircraft shield tests. Three fuel systems were considered, the most feasible of which appeared to be a mixture of UO_2SO_2 dissolved in D_2O. Extensive nuclear calculations

[redacted]

would be required to demonstrate the degree to which such a fuel system would give a nuclear approximation to the molten-salt system proposed for aircraft propulsion.

Equipment is being assembled for calibration and efficiency measurements in preparation for shielding measurements during operation of the ART. In order to conform with the engineering test schedule on the pressure shell, this work must be completed before December 1, 1957.

It is anticipated that the detector for gamma-ray spectroscopic measurements at the ART and the BSF will consist of one large total absorption thallium-activated sodium iodide crystal. Since these large crystals are not commonly in use, the characteristics of a 9-in.-dia crystal are now being investigated.

A housing which includes a tungsten collimator and a lithium-lead shield is to be fabricated for the BSF spectrometer. The lithium will be included in a shield in order to avoid background effects caused by neutron radiative capture in the materials of the sodium iodide crystal which is to be used as a spectrometer. The inner cavity of the housing will be lined with a layer of Li^6D to further reduce activation by resonance neutrons. A positioner is being developed which will support the 15-ton assembly and allow the spectrometer collimator to be positioned to within 1 cm of any desired point in the pool at an angle known to within a fraction of a degree.

A 4-cm^3 ion chamber designed for measuring gamma-ray energy deposition in graphite in a high-intensity field, such as that which would be encountered in a radiation damage facility, was tested and calibrated. For these tests the BSF reactor was operated at 200 kw. Plots of measurements taken with this chamber agree in shape with those of earlier measurements made with other detectors for distances out to 240 cm from the reactor.

In order to accurately perform calculations for reactors in which beryllium is used as the reflector or moderator, the neutron diffusion coefficient of beryllium must be known. Equipment is now being fabricated for an experiment which will utilize the "pulsed-neutron method" to determine this coefficient as a function of temperature. This is not computable because various crystal changes take place in beryllium at elevated temperatures which are not well understood. Preliminary experiments will be performed with cubes of graphite, which is also expected to exhibit marked crystal modifications.

Design and development of a UO_2–stainless steel reactor for the BSF are underway. The proposed reactor, which will have a higher-energy gamma-ray spectrum that will more nearly correspond to the leakage spectrum of the ART, will have a near-cubical design that will be amenable to shield tests. The control system will utilize plate-type control devices which will provide the desired nearly symmetrical leakage flux. Several development experiments for the control system have been performed. In addition, heat transfer and reactivity calculations have been carried out. Several experiments have also been performed in the present BSF uranium-aluminum reactor to determine the effects of inserting stainless steel or boron-loaded aluminum plates within the core. The results of these measurements are being used to predict the control that can be effected in a UO_2–stainless steel core.

Part 6

ADVANCED POWER PLANT DESIGN

S. J. Cromer

AIRCRAFT SHIELDING

E. P. Blizard

6.1. ADVANCED POWER PLANT DESIGN

A. P. Fraas

A NUCLEAR-POWERED TRANSPORT TYPE OF AIRCRAFT WITH TURBOPROP ENGINES

W. T. Furgerson J. A. Boppart[1]

A preliminary investigation has been made of the feasibility of using a reflector-moderated circulating-fuel reactor of the ART type in conjunction with turboprop engines to power a transport type of airplane with a currently flying airframe configuration. It was specified that the aircraft was to have sufficient payload capacity to make it readily adaptable to a wide variety of useful applications, including logistics transport, radar picket, and missile launching.

Results of the study indicate that the gross weight of such an aircraft, exclusive of payload, would be approximately 230,000 lb, with shielding sufficient to limit the maximum crew compartment dose rate to 0.02 rem/hr. An aircraft with the Douglas C-133A airframe could carry a payload of from 25,000 to 50,000 lb in all-nuclear-powered flight that would duplicate the present C-133A chemical-powered performance. The required reactor power would be approximately 75 Mw.

Two things became immediately obvious in this investigation. First, since the reactor, shield, and liquid-metal handling equipment would weigh approximately 100,000 lb, the aircraft gross weight should be in the 200,000- to 300,000-lb range and would require a minimum of approximately 50,000 lb of thrust for takeoff. Second, the only way to get thrusts of such magnitude with 60 to 100 Mw of power is with a turboprop. It would take approximately 250 Mw to get the same minimum thrust with a turbojet cycle.

It did not appear that a nuclear cruise propulsion system with chemical augmentation for full power would result in a lighter over-all weight. A reactor shield combination rated at 60 Mw with 0.02 rem/hr in the crew compartment would weigh approximately 89,000 lb. A 30-Mw system would weigh approximately 82,000 lb, and thus only 7000 lb would be available to divide between fuel and fuel-handling equipment. Also, a reactor sized for nuclear cruise only would be run for extended times at full power, whereas a larger reactor designed to give full takeoff power would be operated derated most of the time. If the aircraft carried a reactor capable of supplying cruise power only, it would be restricted to those maneuvers which could be performed at cruise-power setting unless augmentation could be obtained from chemical fuel. This would impose undesirable restrictions on operation of the aircraft. In addition, it is doubtful whether the "nuclear-cruise-only" aircraft could sustain flight with one or more engines out without chemical augmentation. It is not possible to evaluate these factors on a weight basis, but they should be considered. This study was limited on the basis of these considerations to systems having turboprop engines and all-nuclear-powered operation capability. A reactor with sufficient power for takeoff would have sufficient power for maneuvers, and yet it would operate most of the time in its cruise-power range.

Airframe

In the selection of an airframe for conversion to reactor-turboprop propulsion, the following factors were considered:

1. The airframe should be one designed for turboprop engines.
2. The airplane should have a present gross weight, configuration, and payload such that the reactor could be installed with a minimum of airframe structural modification and such that a payload of at least 20,000 lb would be available in addition to the nuclear power-plant weight.
3. The airplane landing gear configuration should be such that landing gear modifications required by the increased landing weight of the nuclear airplane could be accomplished with minimum weight penalty.

The Douglas C-133A airplane appeared to be the only existing airplane which could meet these requirements. No other airplane which is flying at the present time has the required load-carrying capacity and cargo-hold size. The C-133A is a high-wing monoplane logistic transport, with four wing-mounted turboprop engines. An important feature is the short-extension landing gear, which is housed in bulges on the lower sides of the fuselage. The C-133A landing gear is designed for a landing at the maximum gross weight at a

[1]On assignment from Airesearch Mfg. Co.

5 ft/sec descent rate. Pertinent data on the airplane are presented below:

Over-all length	153 ft
Over-all wingspan	180 ft
Maximum gross weight	282,000 lb
Normal gross weight	255,000 lb
Empty weight	109,417 lb
Power plant: (four used)	
Type	Turboprop
Designation	P&W T-34-P3
Rated power	5700 eshp
Weight (less tailpipe)	2564 lb
Fuel capacity	16,000 gal

The weight of the empty airframe without engines is therefore approximately 99,000 lb. On the basis of the maximum and normal gross weights quoted above, there is available approximately 156,000 to 183,000 lb to be divided among engines, reactor and shield, structural modifications, and payload.

It is envisioned that, in the reactor-turboprop-powered C-133A, the reactor and its shield would be installed in the present cargo deck slightly aft from the wing. This would place the reactor directly over the present landing gear and thus tend to minimize the structural modifications required. The engines would be mounted in the wings at approximately the same locations as the present engines.

A further airframe modification, which would be of particular interest during the developmental flying phase, would be the inclusion of chemical engines in addition to the nuclear-powered engines. These engines would be included primarily as a safety measure to provide all-chemical-powered cruise capability. It is believed that four J-47 turbojet engines in B-47-type pods, such as those used on the late-model B-36 bombers, would be appropriate. Since these engines would be operated only in the case of a reactor shutdown, the weight penalty for chemical fuel could be minimized by using chemical fuel instead of water for neutron shielding around the reactor. With the reactor shut down, neutron shielding would not be required, and the chemical fuel could then be drained off to supply the jet engines.

Engines

The turboprop engines for the reactor-turboprop-powered C-133A were designed for a rated power of 5700 eshp each at sea level, equal to that of the present chemical engines. The engines consist of an axial-flow compressor, a liquid-metal-to-air heat exchanger, which takes the place of the combustor in a conventional gas turbine engine, a turbine to drive the compressor, and a second turbine coupled to a gear box for work output. Finally, a variable-area convergent nozzle is installed in the tailpipe.

Engine performance data were adapted from a previous parametric study of a turbojet cycle using hot NaK for heat input.[2] In that study the parameters varied were:

1. airplane altitude,
2. flight Mach number,
3. over-all ram-compressor pressure ratio,
4. NaK maximum temperature,
5. radiator inlet air weight velocity,
6. radiator depth in air flow direction.

Impulse (thrust per unit air flow) was reported as a function of these variables.

For the turboprop engine analysis, the values of specific impulse were translated into propulsion power. The liquid metal temperature was fixed at 2000°R, which was considered a reasonable maximum for current circulating-fuel reactor technology. Radiator depth was fixed at 2 ft, and the compressor pressure ratio was set at 6.0, because these values appeared from the previous study[2] to be near optimum in the low-to-medium altitude range.

Engine configurations were then calculated for the sea-level-static design point for varying values of G, the air flow per square foot of radiator inlet face area. Required engine-air-weight flow, required heat input, engine weight, and radiator weight were determined. Performance for each of these engine configurations was then estimated at altitudes of 18,000 and 36,000 ft and at Mach numbers from 0 to 0.9, with the air flow rates varying as functions of the atmospheric air density and flight Mach number.

The results of this analysis are presented in Figs. 6.1.1 through 6.1.4. As may be seen, the engine-radiator combinations designed for $G = 10$

[2] W. H. Sandeford, *A Parameter Study of the Performance of Nuclear-Powered Turbojet Aircraft Using a Liquid-Metal Heat-Transfer Medium*, ORNL CF-55-8-198 (Aug. 1955).

at sea-level static yield maximum power at altitude, require minimum air flow rate and minimum heat input, and yield minimum engine-radiator weight. Therefore, $G = 10$ at sea-level static was taken as the design value for the engine radiator.

In the previous study on which this analysis was based, an allowance of 9.6% of the engine power output was made for auxiliary power requirements.

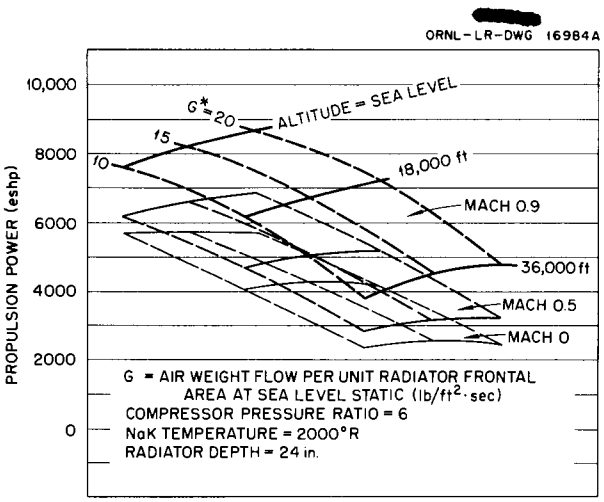

Fig. 6.1.1. Engine Parameter Analysis of Propulsion Power Required for Reactor-Turboprop Propulsion of a Douglas C-133A Aircraft.

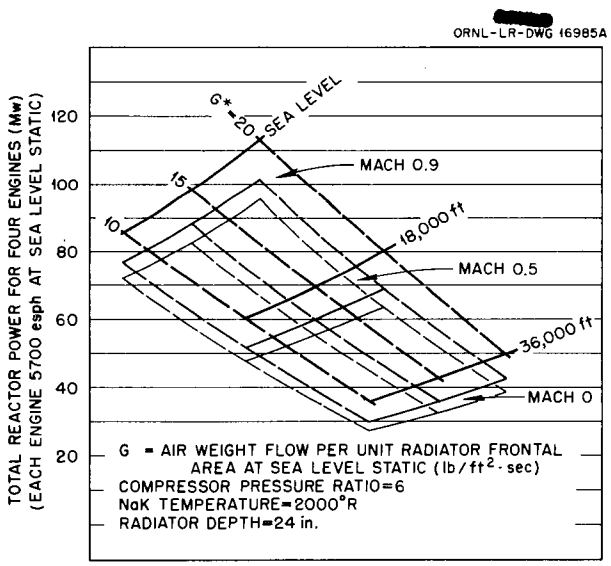

Fig. 6.1.2. Engine Parameter Analysis of Reactor Power Required for Reactor-Turboprop Propulsion of a Douglas C-133A Aircraft.

This allowance was retained in the present analysis.

A preliminary engine design was calculated in order to obtain size and weight, and details of the components as tentatively envisioned are described below: The compressor consists of ten axial-flow stages that give an over-all total pressure ratio of 6. The tip diameter is constant at 24 in. Design speed is 9550 rpm. Hub diameters vary from 15 in. at the inlet to 21 in. at the discharge. Work input is constant from hub to tip and equal for the ten stages. The first stage is transonic at the rotor tip. A small amount of prerotation in free vortex form is used to give an absolute circumferential velocity component of 75 ft/sec entering the rotor tip. The use of such prerotation reduces the diffusion factor at the first-stage rotor hub and helps to effect an even distribution of flow over the inlet annulus. If efficiencies that vary from 0.90 at the first stage to 0.88 at the tenth stage are assumed, the resulting over-all compressor efficiency is expected to be approximately 0.86.

The liquid-metal-to-air heat exchanger is of the plate-fin type. Depth in the direction of air flow is 24 in., and the frontal area perpendicular to air

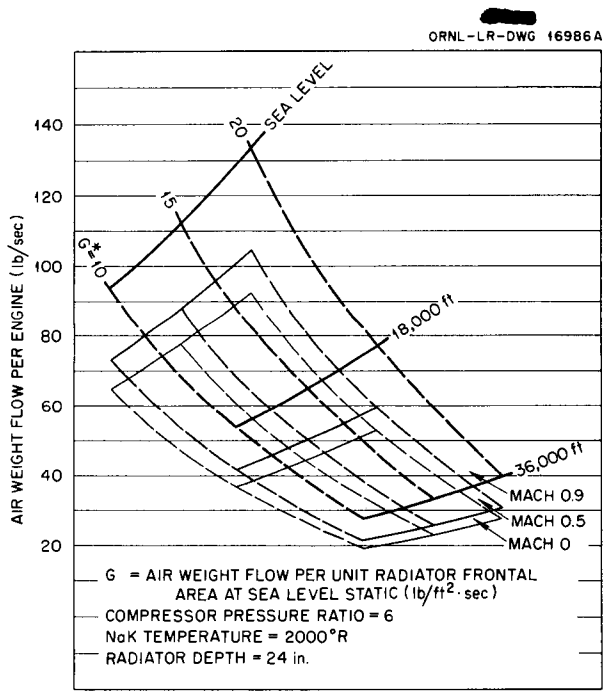

Fig. 6.1.3. Engine Parameter Analysis of Engine-Air-Weight Flow Required for Reactor-Turboprop Propulsion of a Douglas C-133A Aircraft.

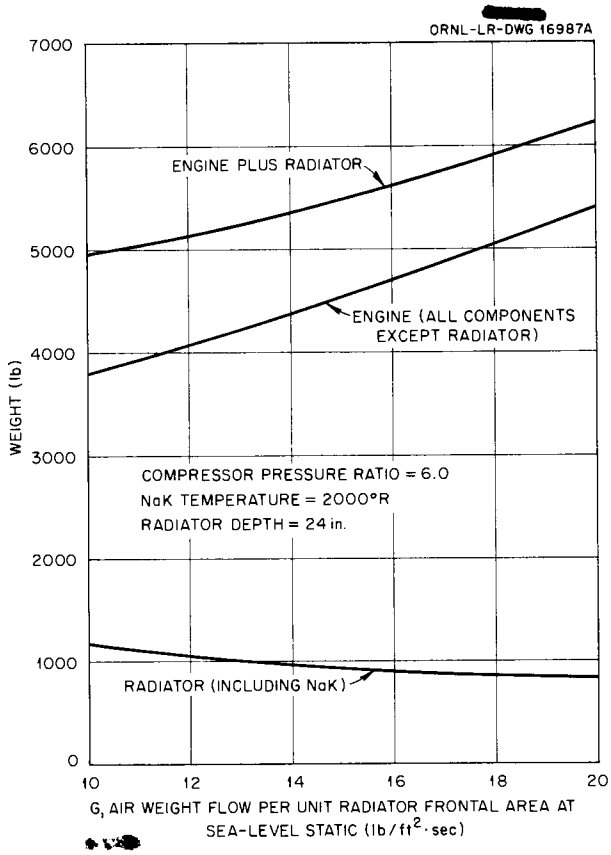

Fig. 6.1.4. Engine Parameter Analysis of Engine and Radiator Weights Required for Reactor-Turboprop Propulsion of a Douglas C-133A Aircraft.

flow is 6.5 ft^2. Since for this type of engine the minimum frontal area is not a prime consideration, the heat exchanger is in a square configuration in order to achieve the greatest simplicity of design. Air temperature leaving the radiator is 1930°R.

As mentioned previously, the turbine section of the engine is separated into two parts: one turbine is used to drive the compressor and a second provides the output work. While this "free turbine" design introduces some weight and mechanical complexity, it is preferred for a number of reasons. First, the power turbine can run at varying speeds with a minimum variation in compressor speed. Second, during a landing approach the compressor section can run at maximum speed. The propellers would be in flat pitch with their speed controlled by the back pressure exerted by a variable area nozzle on the power turbine. In the event of a missed approach, thrust could be obtained without waiting for the compressor section to accelerate. Third, windmilling of a dead engine would not create the drag which results when the compressor is rotated. Finally, an aircraft on the ground could brake its propellers and allow the compressor sections to run for afterheat removal or accessory drive. The compressor turbine has 9.6% excess capacity to allow for extraction of accessory power, which allows a full 5700-hp output from the power turbine. Both the compressor and the power turbine are single-stage axial-flow types, with a constant tip diameter of 27 in.

It should be noted that this is essentially a derated engine. A turbine inlet temperature of 1930°R corresponds approximately to cruise conditions on most turbine engines. The engine should therefore be able to operate at full takeoff power for extended periods.

Consideration has been given to the possibility of modifying an existing engine design for use with nuclear power. However, since the radiator pressure drop is higher than that of a combustion engine and the turbine inlet temperature is lower, the propulsion power per unit air weight flow per second (horsepower per pound of air per second) is appreciably lower in nuclear-powered engines than in chemically powered turbine engines. Therefore, the air-handling capacity of the nuclear-powered engine must be larger than that of the T-34 engines installed in the C-133A. No turboprop engines are known which have the required air-handling capacity. In any event, the practicability of making such a modification is questioned.

There exists a widespread belief that a chemical engine can be converted to run with nuclear heat simply by replacing the combustion chamber with radiators. Unfortunately, such is not the case. The components of a turbine engine are closely coupled both mechanically and aerodynamically. Consequently, alteration of any one component can be expected to have a profound effect on the operation of the others. For instance, the fact that the radiator pressure loss is higher than that of a typical combustion chamber will result in a mismatch between the compressor and turbine of a chemical engine. Also, the lengthening of the compressor drive shaft to provide room for the radiators would entail the risk of problems with critical speed. It is therefore believed that a new engine should be designed specifically for this application.

It is emphasized that the required engine is not an advanced design. The relatively low temperature level at which heat is available from the liquid metal results in low compressor-pressure ratio requirements. Since the radiator will require approximately 6.5 ft^2 of frontal area, there is no need to design the compressor for high flows per unit frontal area.

The engine can therefore be simple aerodynamically. Such refinements as twin-spool designs or variable-pitch stators are not needed and, indeed, are not desirable. The inlet hub-tip ratio can be conservative at 0.6 to 0.65. With the exception of the radiators, the design of such an engine would involve only well-established information.

In the interest of simplicity it is felt that the engine should be designed to run on nuclear heat alone rather than with chemical augmentation. The use of separate conventional chemical jet engines for an emergency power source would result in less complication of the engines and their control system.

Reactor and Reactor Shield

The reactor is a reflector-moderated circulating-fuel type. Reactor and shield design data are taken from a previous study.[3] The reactor power required for four engines was found, from Fig. 6.1.2, to be about 75 Mw. The reactor core diameter was set at 21 in. as a compromise between compactness and desirable fuel properties. By extrapolating from the ART, the weight of the reactor plus intermediate heat exchangers, pressure shell, etc., is estimated to be 14,000 lb.

Several reactor shields were designed to yield doses of from 2.5 to 12.5 rem/hr of radiation from the reactor at the crew compartment, which was assumed to be 50 ft from the reactor center. The dose from the reactor was designed to be 10% neutrons and 90% gamma rays. Weights of reactor and shield as a function of dose at the crew shield are plotted in Fig. 6.1.5.

Crew Shield

The dose at the crew shield was assumed to be that due to radiation from the reactor plus 2.5 rem/hr of gamma radiation from activated sodium

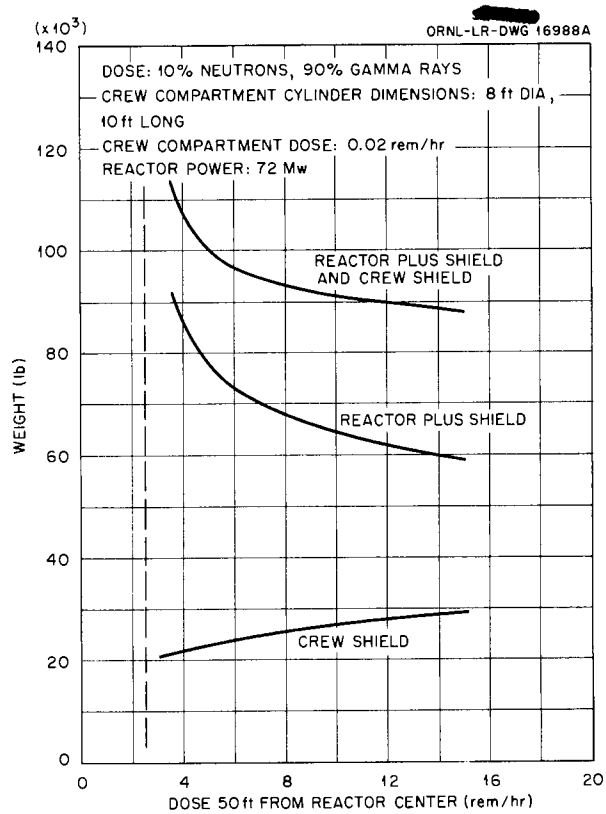

Fig. 6.1.5. Reactor and Shield Weights as a Function of Dose at Crew Shield of a Reactor-Powered C-133A Aircraft.

in the NaK pipes and engine radiators. This figure for sodium radiation is based upon the degree of sodium activation anticipated in the ART. It appears that this activation can be reduced by a factor of 5 to 10 with little weight penalty by more careful shielding between the reactor core and the heat exchanger.[4] Thus, the use of the 2.5 rem/hr for sodium radiation at the crew shield introduces a considerable degree of pessimism into the analysis. No shielding was provided for the NaK lines and radiators, since flight shielding is more economically accomplished by the crew shield. The NaK lines and radiators can be drained to reduce radiation to tolerable levels on the ground.

Considerable reduction in the activity of the secondary fluid circuit might be realized by substituting potassium for the NaK. Both calculations and tests indicate that the activity of the potassium should be lower than that of NaK by about a

[3] E. P. Blizard and H. Goldstein (eds.), *Report of the 1953 Summer Shielding Session*, ORNL-1575 (June 14, 1954).

[4] A. M. Perry, private communication.

factor of 20. Another factor of perhaps 5 could be obtained through the use of B^{10} in place of natural boron for protecting the heat exchanger (at a cost increase of perhaps $100,000). Thus the total activity in the liquid-metal circuits could be reduced to 5 or 10 curies (and there would be some self-shielding, especially in the radiators). The gamma rays from potassium are 1.5 Mev rather than 2.5 Mev, as is the case for sodium.

The melting point of potassium is 144°F, and its specific heat is somewhat lower than that of NaK so that the required flow rate is higher. If the NaK were replaced with potassium and all other weights remained the same, the added weight would be 3000 lb. However, if sufficient shielding were added to the system in which NaK was used to give the same crew dose that would exist with potassium, the weight with potassium would be less than the weight with NaK.

The crew compartment was assumed to be a cylinder 10 ft long and 8 ft in diameter. Crew shields were designed for each value of incident radiation encountered over the range of reactor shield weights to provide a dose inside the crew compartment of 0.02 rem/hr. Crew shield weights were found from a previous study[5] and are plotted in Fig. 6.1.5.

Chemical Auxiliary Engines

The addition of two B-47-type pods (two G-E J-47 engines each) to the nuclear C-133A airframe would provide sufficient power to cruise on chemical engines alone with the reactor shut down. The J-47 engines weigh approximately 2500 lb each; the installed weight for four engines is estimated to be 14,000 lb.

The reactor shield designed for 2.5 rem/hr reactor radiation dose at the crew shield contains approximately 32,000 lb of water. If this is replaced with chemical fuel, a cruise duration of approximately 1 hr on chemical power only would be provided. Additional chemical fuel capacity could be obtained by installing other fuel tanks at the expense of a decrease in payload.

Weight and Payload Estimates

The estimated weights of the components and accessories of the nuclear powerplant, together with airframe weights, are listed below (based on a total dose of 10 rem/hr at 50 ft from the reactor).

	Weight (lb)
Airframe, less engines	99,161
Engines: 4 at 4270 lb	17,080
Radiators: 4 at 1297 lb	5,188
NaK piping	3,429
Reactor (including intermediate heat exchanger, pressure shell, fuel pumps, etc.)	14,000
NaK pumps and drives	6,000
Reactor shield	48,000
Crew shield	27,000
Increase in structural weight	10,000
Empty weight of nuclear-powered C-133A	229,858
Installed weight of four J-47 engines	14,000
Empty weight of C-133A aircraft plus nuclear power plant and auxiliary chemical engine	243,858

Based on the previously quoted values of maximum gross weight and normal gross weight for the C-133A, the available payloads are estimated as follows:

	Maximum Payload (lb)	Normal Payload (lb)
C-133A with nuclear power	52,142	25,142
C-133A with nuclear power and auxiliary chemical power	38,142	11,142

[5] E. P. Blizard and H. Goldstein (eds.), *Report of the 1953 Summer Shielding Session*, ORNL-1575, Fig. IV-I-8, p 376 (June 14, 1954).

6.2. TOWER SHIELDING FACILITY

C. E. Clifford

IRRADIATION OF A PRATT & WHITNEY AIRCRAFT J-57 ENGINE

W. J. McCool[1] F. J. Muckenthaler

A Pratt and Whitney Aircraft J-57 model jet engine was operated continuously for 50 hr while it was exposed to a total tissue dose of 7×10^8 ergs/g from the Tower Shielding Facility (TSF) reactor in order to test the compatibility of a jet engine and a reactor system. The objectives of the experiment were to study the effects of radiation on the control and performance of the engine, the radiation damage to engine components, and the induced radioactivation of the engine. Gamma-ray spectra and dose-rate measurements were taken at various positions around the engine immediately after exposure and for several days following shutdown. A description of the experiment is presented below.

Experimental Arrangement During the Irradiation

The experimental geometry for the irradiation of the engine is shown in Figs. 6.2.1 and 6.2.2. The front face of the TSF reactor was positioned 13 cm from the wall of the reactor tank. The reactor center was 8.5 ft from the axis of the engine at the nearest point, and both were 7.3 ft above ground level. In order to reduce the thermal-neutron flux incident upon the engine, a ½-in.-thick boral shield was inserted between the reactor and the engine (Fig. 6.2.1). A heavy blast shield was placed between the engine turbine section and the reactor controls to prevent damage in case of explosion. The controls of the engine were operated by cables from a control panel located in the TSF control room, and both the engine and the reactor were monitored by television cameras. The engine was mounted on a sled which could be moved in case of an emergency or on termination of the experiment.

[1]On assignment from Pratt & Whitney Aircraft.

[redacted]
2-01-056-19-D-529

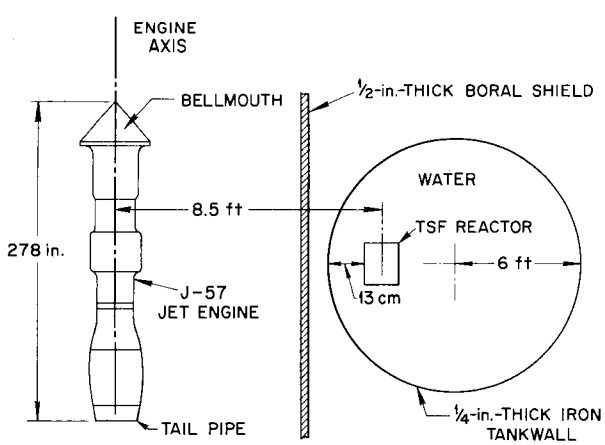

Fig. 6.2.1. Geometry for J-57 Jet-Engine Irradiation at TSF (Top View).

Gamma-Ray and Neutron Dose-Rate Measurements Preceding and During the Engine Exposure (Phases I and II)

Before the irradiation of the engine, dose-rate measurements were taken along a line which coincided with the axis of the engine when it was placed in position. The results of these measurements (Phase I measurements) are plotted in Figs. 6.2.3 through 6.2.6 as a function of the distance from the tailpipe, the total length between the afterburner and the bellmouth being 278 in. Figures 6.2.3 and 6.2.4 show the low-energy neutron distribution as measured by a fission chamber and gold foils, respectively. The fission-chamber measurements were taken to obtain the lateral distribution of low-energy neutrons; the cadmium difference technique was used with gold foils. Neutron dose-rate measurements with a Hornyak button are plotted in Fig. 6.2.5, and corresponding gamma-ray dose rates detected with a 50-cm^3 graphite ion chamber are shown in Fig. 6.2.6.

Phase II measurements were made with both the engine and the reactor in position. Threshold detectors[2] consisting of Pu^{239}, Np^{237}, U^{238}, and sulfur were used at various positions on the surface of the engine to obtain the neutron flux above

[2]G. S. Hurst *et al.*, *Rev. Scientific Instr.* **27**, 153-156 (1956).

Fig. 6.2.2. TSF Reactor and J-57 Jet Engine in Operation Position.

6.0 kev, 0.75 Mev, 2.9 Mev, and 1.5 Mev, respectively (Fig. 6.2.7). The neutron flux thus obtained at various energy thresholds was used with the tissue dose curve[2] to calculate the integrated equivalent neutron tissue dose received by the engine at various points (Table 6.2.1). Gold wires were also placed on the surface of the engine on both the side next to the reactor and the side opposite from the reactor. These wires, which were in the same horizontal plane as the engine axis and were wrapped with cadmium foils at 6-in. intervals, were in place during the entire engine exposure to obtain the low-energy (<5 ev) neutron distribution (Figs. 6.2.8 and 6.2.9). It may be noted that the data of Figs. 6.2.8 and 6.2.9 have not been normalized to unit power. The peaks found in Figs. 6.2.8 and 6.2.9 were caused by the moderation of higher-energy neutrons by fuel and/or lubricant in the vicinity of that portion of the wire.

Gamma-Ray Dose-Rate Measurements After Engine Exposure (Phase III)

Measurements of the gamma-ray dose rate from the engine were taken after the engine was removed from the vicinity of the reactor (Fig. 6.2.10). These measurements were made with a cutie-pie survey type of hand ion chamber at various points around the engine for periods varying from 1 hr up

to several days after shutdown of the reactor. A concrete-block wall was built on the ground near the engine (see Fig. 6.2.10) to shield out, insofar as possible, the gamma rays emanating from the sled upon which the engine was mounted. Gamma-ray dose-rate measurements were made on the surface of the engine at the points marked in Fig. 6.2.10. The induced gamma-ray dose rate along the axis of the engine was considered to be proportional to the neutron dose received at each opposite surface point; the point opposite the center of the reactor (No. 16) had the highest dose

[redacted]

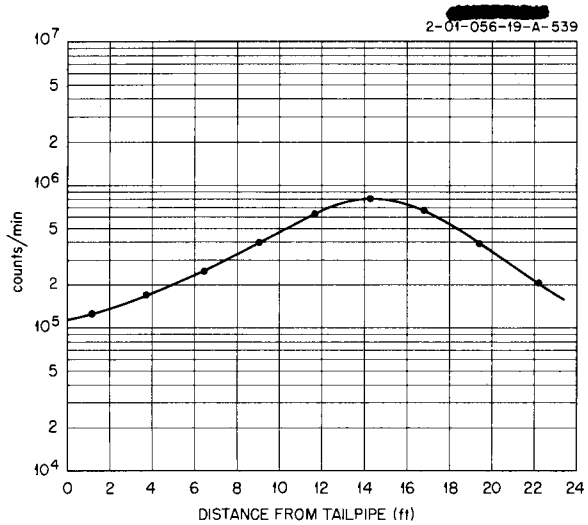

Fig. 6.2.3. Fission-Chamber Measurements of the Neutron Distribution Along a Line Coincident with the J-57 Engine Axis (Phase I, Engine Not Present).

[redacted]

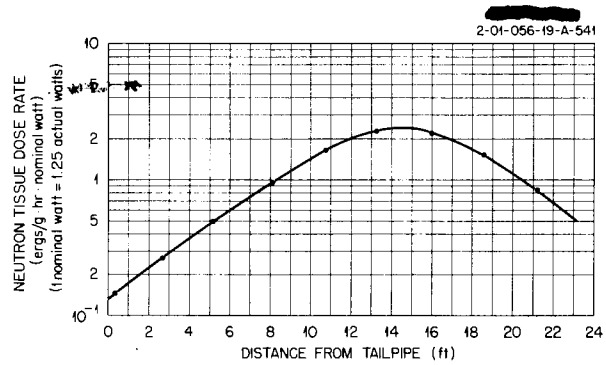

Fig. 6.2.5. Hornyak-Button Measurements of the Neutron Dose Rate Along a Line Coincident with the J-57 Engine Axis (Phase I, Engine Not Present).

[redacted]

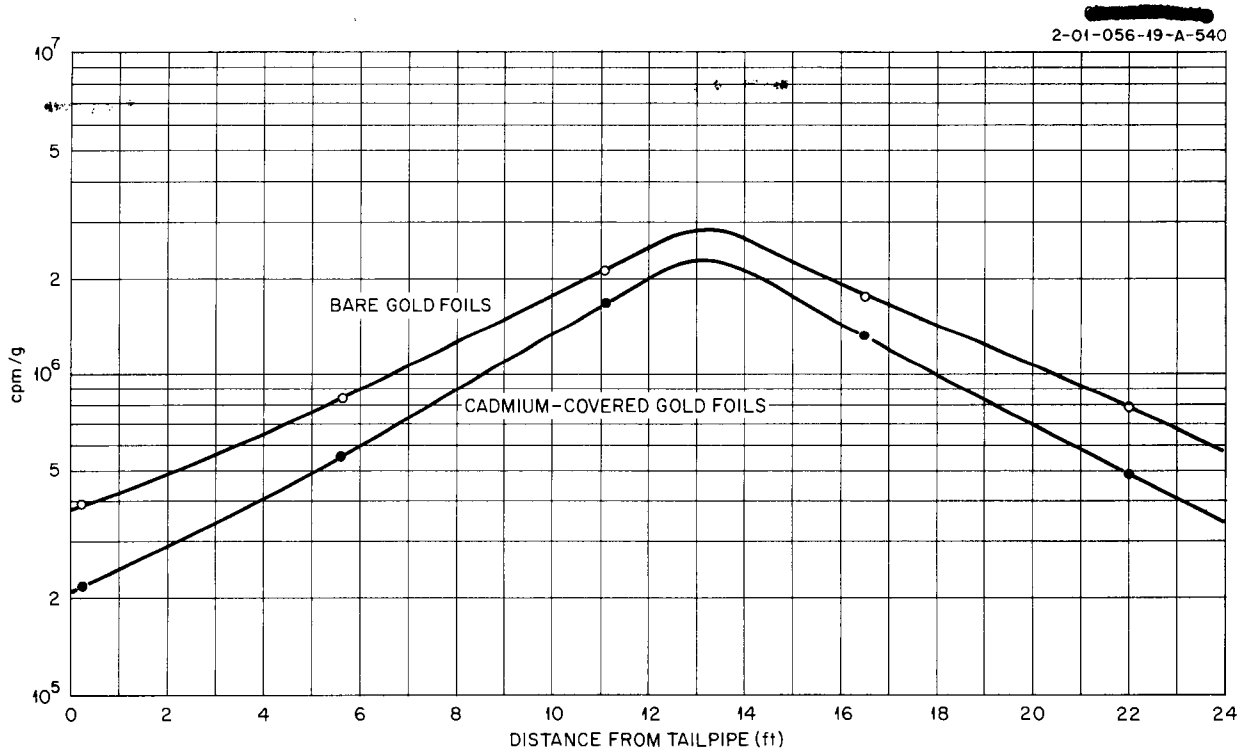

Fig. 6.2.4. Gold-Foil Measurements of the Neutron Distribution Along a Line Coincident with the J-57 Engine Axis (Phase I, Engine Not Present).

rates. Table 6.2.2 presents a typical set of cutie-pie readings obtained at various times and distances along a normal to the axis of the engine through point No. 16. Since the cutie-pie ion chamber is only a survey type of detector, there is a rather large error in obtaining a dose rate at any specific time or place; however, its versatility makes it possible to obtain many readings at various locations in a short period. A plot of the [redacted]

[redacted]

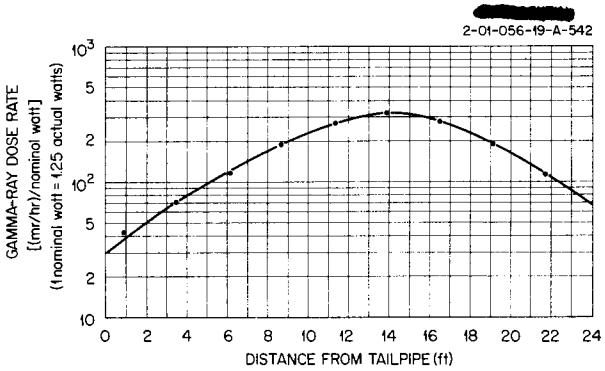

Fig. 6.2.6. Ion-Chamber Measurements of the Gamma-Ray Dose-Rate Distribution Along a Line Coincident with the J-57 Engine Axis (Phase I, Engine Not Present).

Table 6.2.1. Integrated Gamma-Ray and Fast-Neutron Dose Measurements Made During Phases I and II of the J-57 Engine Irradiation Experiment at the TSF*

Distance From Tailpipe (ft)	Gamma-Ray Dose, Ion Chamber, Phase I (r)	Fast-Neutron Dose (rep)	
		Hornyak Button, Phase I	Threshold Detectors, Phase II
	$\times 10^6$	$\times 10^5$	$\times 10^5$
6.33	2.50	1.40	1.34
10.4	4.80	2.27	5.11
13.4	6.39	4.85	8.87
14.7	6.40	5.16	9.60
15.8	5.90	4.95	8.89
18.2	4.40	3.44	5.91
19.1	3.80	2.91	4.76
18.2**			1.58

*Phase I measurements were made before the irradiation along a line corresponding to the engine axis when it was in position. Phase II measurements were made during the irradiation on the surface of the engine.

**Measurement made on side of engine away from the reactor.

[redacted]

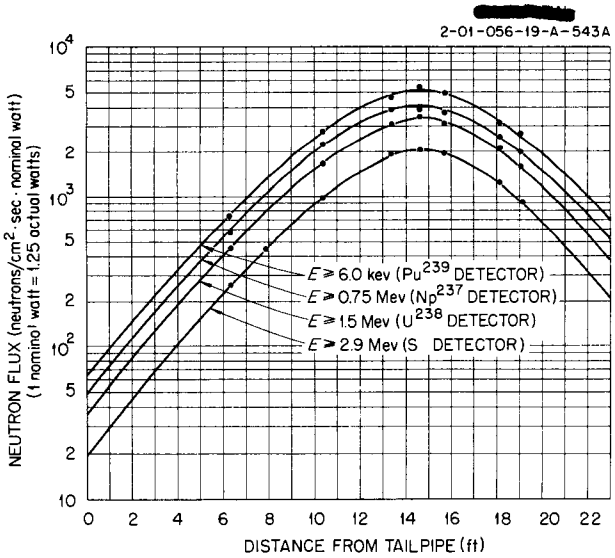

Fig. 6.2.7. Neutron Flux Above Various Energy Thresholds on the Surface of the J-57 Engine Nearest the Reactor During Irradiation (Phase II).

[redacted]

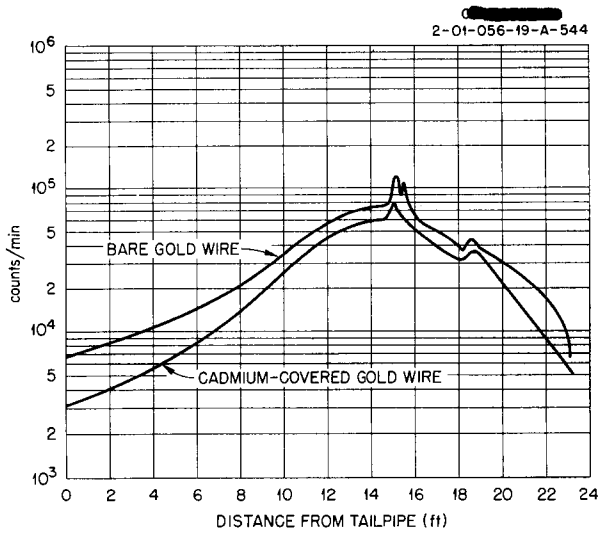

Fig. 6.2.8. Gold-Wire Measurements of the Neutron Distribution on the Surface of the J-57 Engine Nearest the Reactor During Irradiation (Phase II).

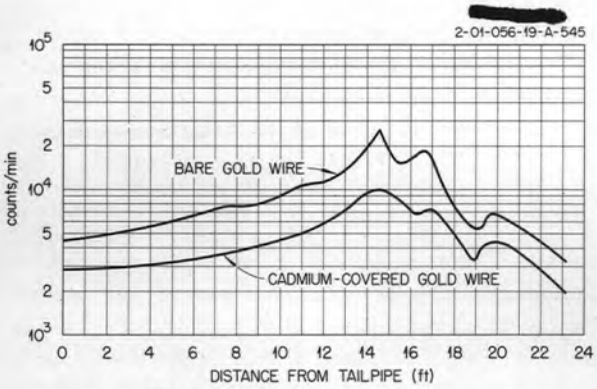

Fig. 6.2.9. Gold-Wire Measurements of the Neutron Distribution on the Surface of the J-57 Engine Farthest from the Reactor During Irradiation (Phase II).

time dependency of these dose rates does give a reasonably accurate estimate of the dose rate at any point at a given time.

Gamma-Ray Spectra Measurements After Engine Exposure (Phase III)

In addition to the gamma-ray dose-rate measurements, an attempt was made to determine the spectrum of gamma rays emitted from the engine after its irradiation. The detector used for these spectra measurements was a 3- by 3-in. sodium iodide crystal which was mounted so that the cylindrical axis of the crystal was coincident with a line that was normal to and bisected the engine axis (see Fig. 6.2.11). The crystal and phototube were enclosed in a lead collimator (Fig. 6.2.12), and a 4-in.-thick lead slab with a window was

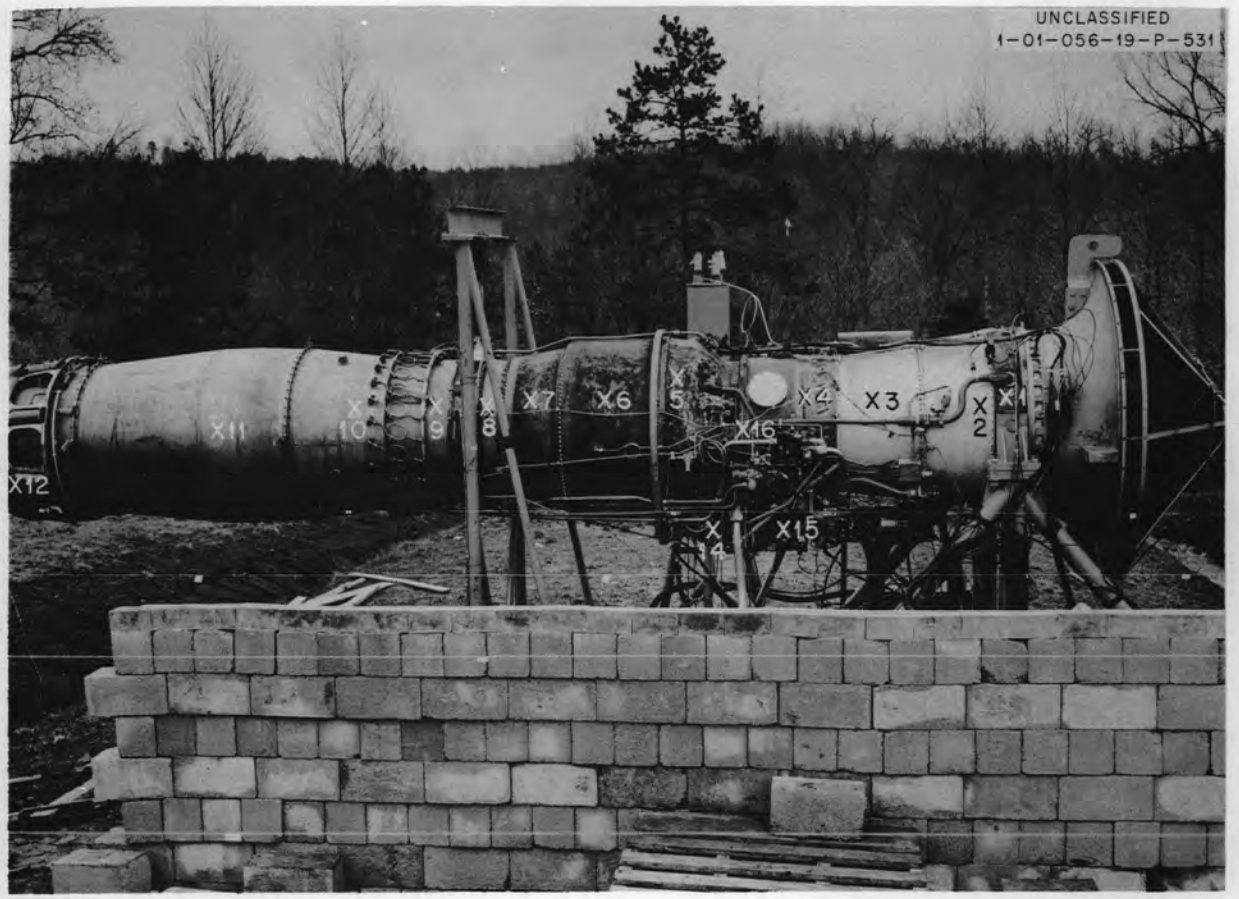

Fig. 6.2.10. Side View of J-57 Engine Showing Surface Points for Gamma-Ray Dose-Rate Measurements.

placed 4 ft in front of the collimator so that only the engine could be seen by the crystal. This reduced to a minimum the contribution to the spectrum from the ground- and air-scattered gamma rays. The sodium iodide crystal was mounted on a DuMont 6363 phototube, and pulses from the phototube were fed through a preamplifier and A-1D amplifier into a 20-channel analyzer.

Table 6.2.2. Gamma-Ray Dose Rates at Various Points from the J-57 Engine at Various Times After Reactor Shutdown*

Date	Time	Gamma-Roy Dose Rate (mr/hr)**					
		Distance from Engine Axis (ft)					
		0	5	10	15	20	25
1-28-57	17:00		800	112	55	30	22
	17:20	3200	780	108	48	24	16
	17:45	2500	640	120	46	25	15
	18:55	1730	560	100	38	20	11
	19:35	1570	480	85	32	14	8
	19:50	1550	420	77	28	15	10
	20:50	1500	380	64	28	17	12
	21:45	780	300	57	22	10	8
	22:40	700	220	44	16	7	
	23:40	700	215	42	19	11	
1-29-57	00:40	720	205	39	16	11	
	01:40	750	120	30	20	12	
	02:40	600	170	26	13	10	
	03:40	600	185	25	18		
	04:40	600	140	25	12		
	05:40	460	100	22	10		
	06:40	460	110	20	8		
	07:40	600	84	21			
	08:40	405	83	17			
	09:40	450	87	20			
	11:40	440	64	10			
	13:40	260	57	16			
	15:40	250	54	10			
	17:40	200	50				
	23:40	150	38				
1-30-57	05:40	110	29				
	11:40	120	20				
	17:40	120	24				
1-31-57	08:40	78	11				

*Reactor shutdown time 1-28-57 at 15:35.

**All measurements were made along a line normal to the engine axis through point 16 shown in Fig. 6.2.10.

The over-all gain of the system was kept constant for each measurement by adjusting either the high voltage or the gain of the A-1D amplifier until the Zn^{65} (E = 1.114 Mev) photoelectric peak appeared at an identical pulse-height setting.

The first spectrum (not presented here) was measured approximately 6 hr after the reactor shutdown. The detector was placed 129 ft from the center of the jet engine in a gamma-ray field of about 1 mr/hr. A total of four spectra was taken at this position at various times after the reactor shutdown and two of these are shown in Fig. 6.2.13. In order to assure that there were no photoelectric peaks at higher pulse-height selector values than the range covered during these measurements, the gain was reduced to one-half the previous value, which extended the energy range covered by a factor of 2 (Fig. 6.2.14). The remaining measurements, made at a point 81 ft from the center of the jet engine, resulted in improved counting statistics. Two typical spectra at this separation distance are shown in Fig. 6.2.15. A total of 15 spectrum measurements was taken at the various positions. The spectra plotted in Figs. 6.2.13 through 6.2.15 have the background subtracted. The background was obtained by measuring the gamma-ray spectrum with a 4-in.-thick lead block inserted into the window of the lead slab in front of the collimator.

The energies of the peaks on the pulse-height spectrum were determined by comparing the response of the crystal to 1.114-Mev Zn^{65} and 2.63-Mev ThC″ gamma rays (Fig. 6.2.16) to the response of the crystal to gamma rays from the engine. The peaks due to gamma rays from Na^{24} (E = 2.76 and 1.38 Mev) and Mn^{56} (E = 2.06, 1.7, and 0.82 Mev) were thus identified. Selection of materials responsible for the low-energy gamma rays (E < 1 Mev) was not so simple. Some help in analysis is provided by a "subtraction method" wherein all the contribution from the highest energy gamma ray in the spectrum is subtracted from the spectrum. The "subtraction" process is then repeated for lower and lower energy gamma rays until the lowest energy measured in the spectrum is reached. This method requires the use of templates for each gamma-ray energy interval. (A template is a spectrum from any initial single-

Fig. 6.2.11. Experimental Arrangement of J-57 Engine and Spectrometer (Extreme Right) for Gamma-Ray Spectrum Measurements.

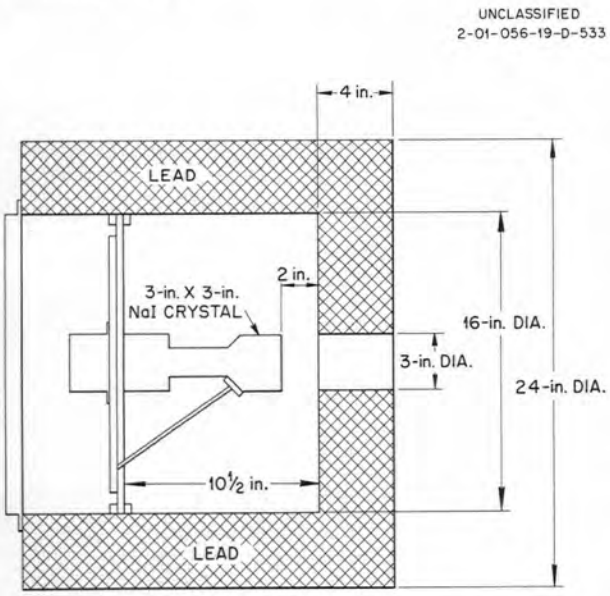

Fig. 6.2.12. Geometry of NaI Crystal and Lead Collimator for J-57 Engine Gamma-Ray Spectra Measurements.

energy-value gamma ray.) Each template should be obtained under detector conditions identical to those used for measuring the unknown spectrum. An analysis of this type is adequate to determine an energy spectrum but not sufficient to give complete identification of the elements responsible, since many elements have gamma rays of approximately the same energy. Since identification of the contributing element is desired, spectra of possible contributing elements have been made. Comparison of these spectra with the spectrum from the engine is now in process. Some of these source spectra are shown in Fig. 6.2.17. Some preliminary subtractions were made on a pulse-height spectrum so that it would be possible to approximate the amount of Na^{24} and Mn^{56} in the jet engine at the time of shutdown. For these calculations, the spectrum taken 11.5 hr after shutdown was used. Results indicate that at the time of shutdown there was 27.2 mc of Na^{24} and 345 mc of Mn^{56} present in the engine.

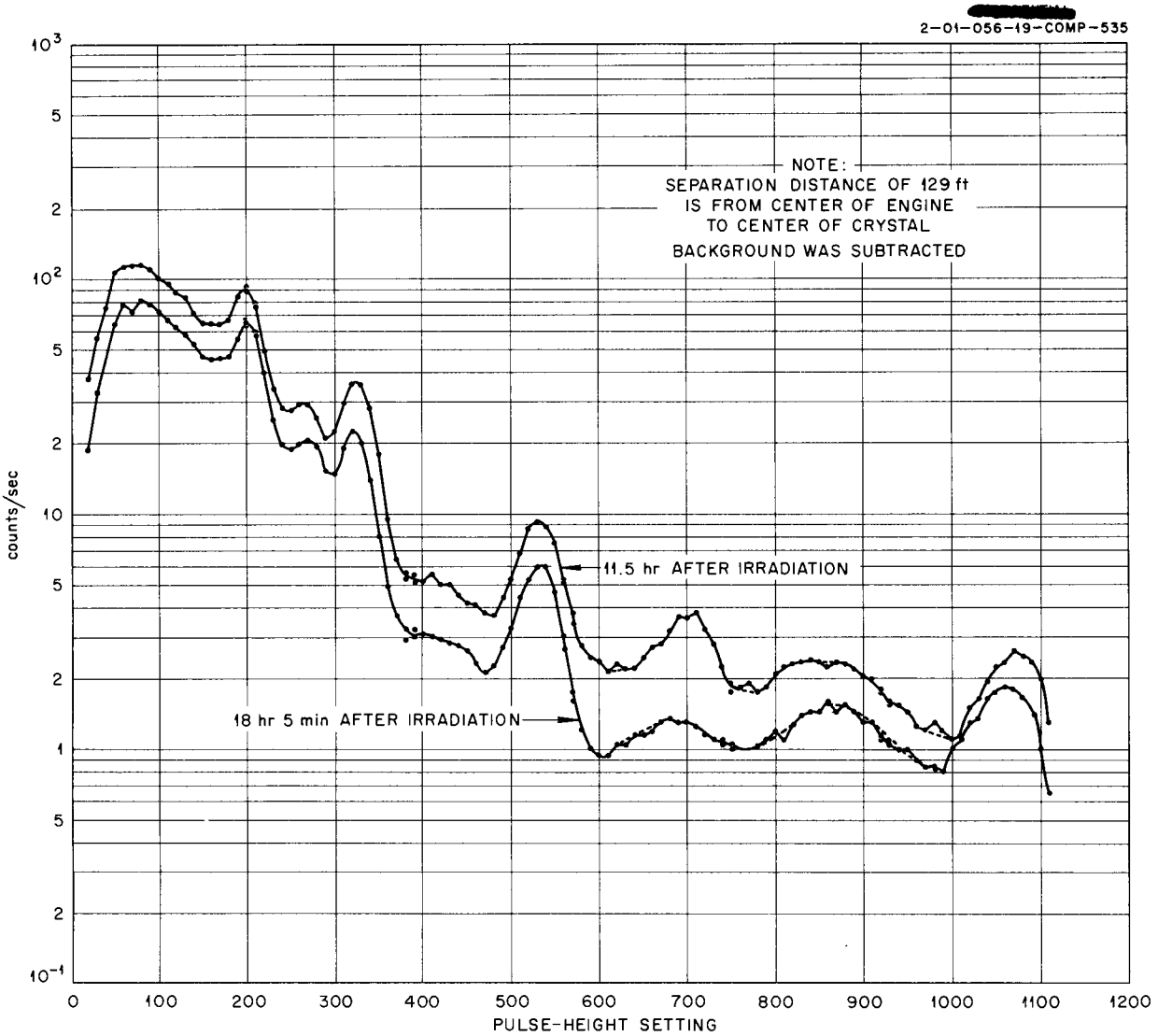

Fig. 6.2.13. Spectra of Gamma Rays 129 ft from the J-57 Engine 11.5 hr and 18 hr 5 min After Irradiation (Gain = 32 × 0.76).

[redacted]

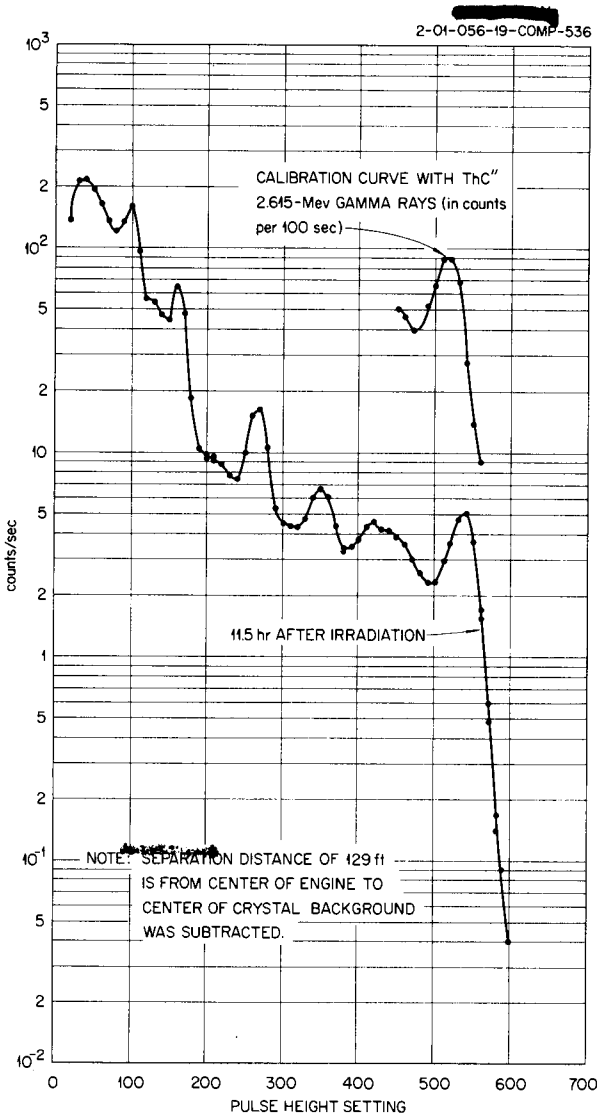

Fig. 6.2.14. Spectrum of Gamma Rays 129 ft from the J-57 Engine 11.5 hr After Irradiation (Gain = 16 × 0.76).

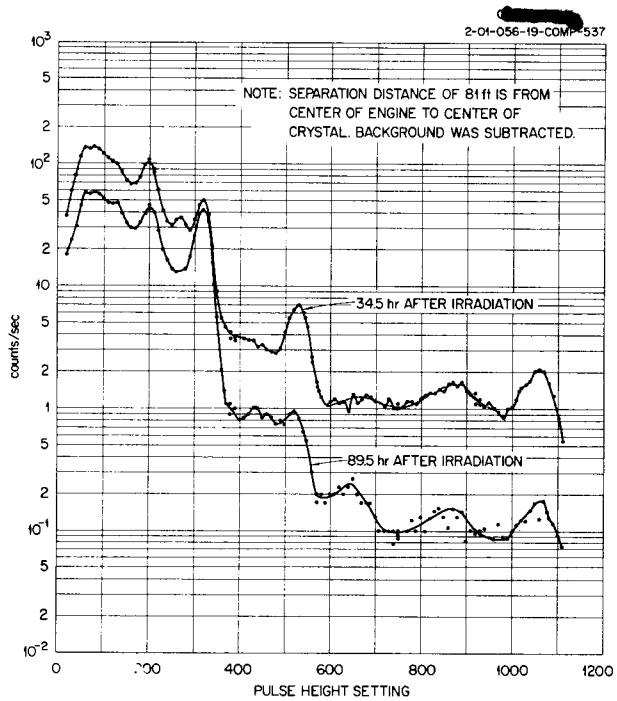

Fig. 6.2.15. Spectra of Gamma Rays 81 ft from the J-57 Engine 34.5 and 89.5 hr After Irradiation (Gain = 32 × 0.76).

Analysis of Results

Analysis of the preceding experimental data will be continued in order to identify the elements which have induced radioactivity. The engine has now been returned to Pratt & Whitney Aircraft for radiation-damage studies. During the experiment no deleterious effects on the performance of the engine were observable.

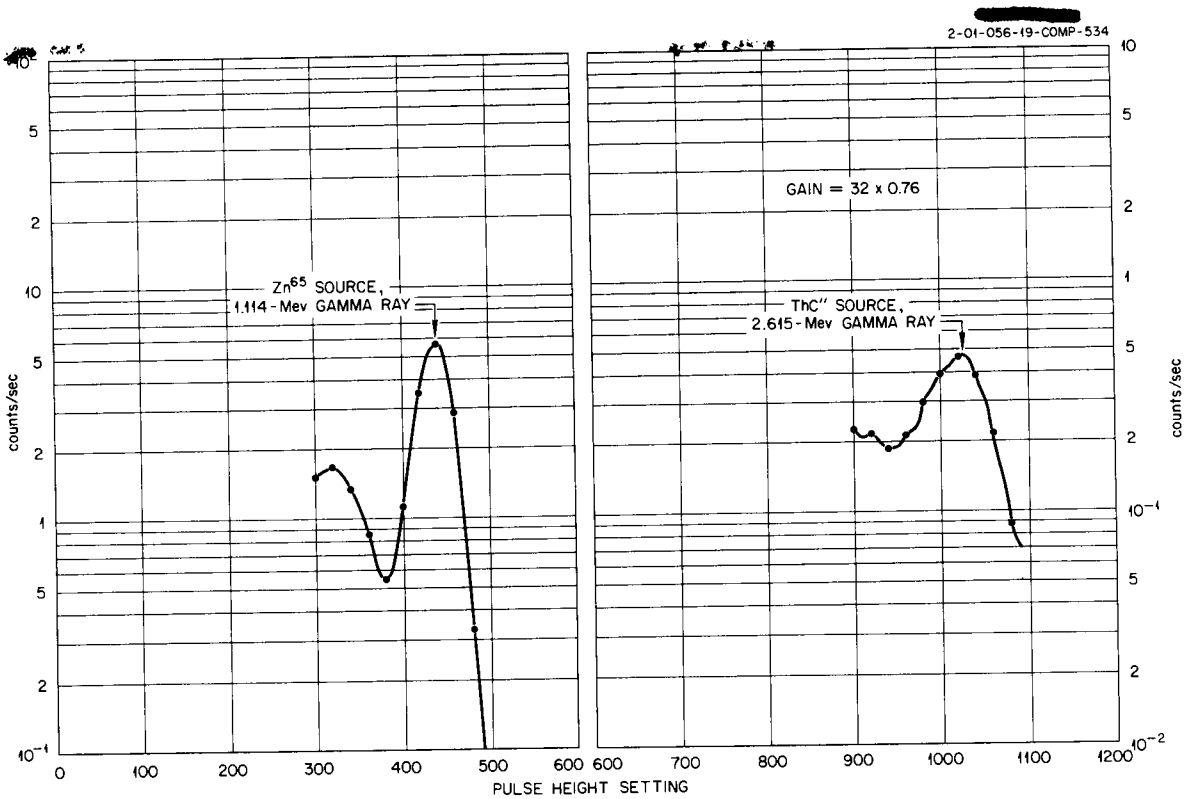

Fig. 6.2.16. Response of Spectrometer to Zn^{65} and ThC'' Gamma Rays.

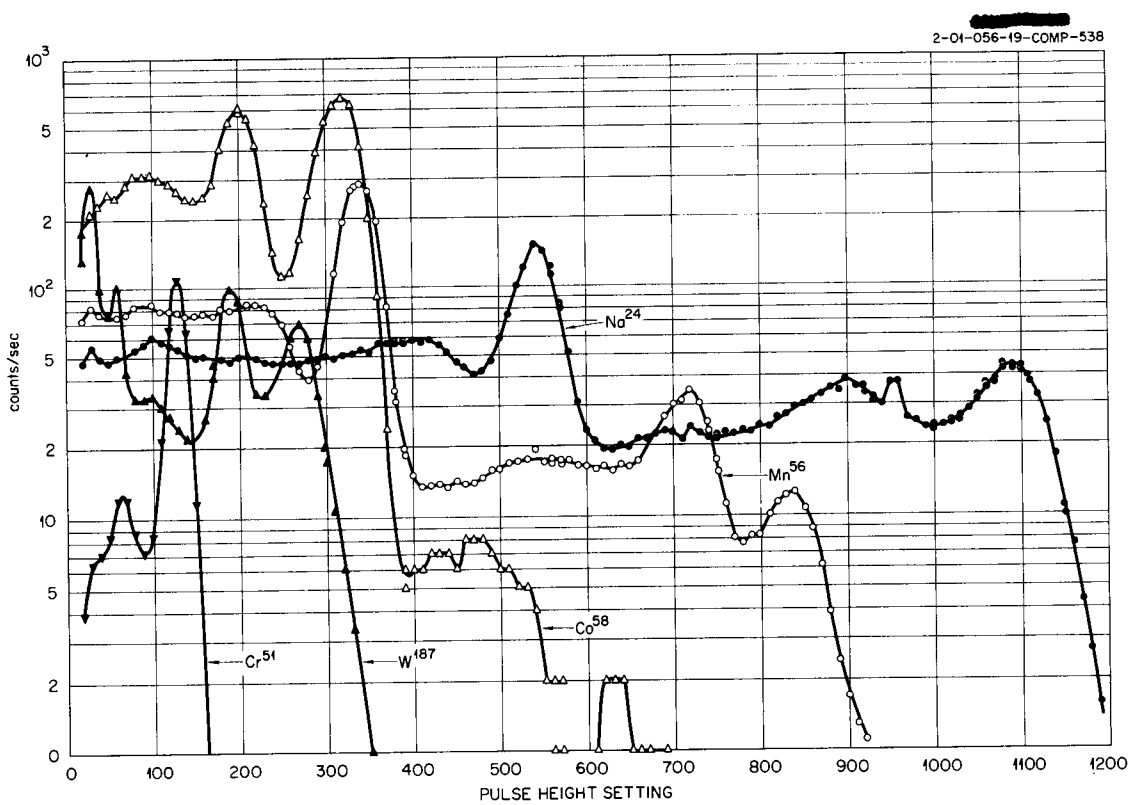

Fig. 6.2.17. Response of Spectrometer to Mn^{56}, Na^{24}, Co^{58}, W^{187}, and Cr^{51} Gamma Rays.

6.3. BULK SHIELDING FACILITY

F. C. Maienschein

PRELIMINARY MEASUREMENTS OF THE SPECTRUM OF PROMPT GAMMA RAYS FROM THERMAL FISSION OF U^{235}

F. C. Maienschein R. W. Peelle
T. A. Love

Prompt gamma rays, that is, those that are emitted after fission without measurable delay, are present in every fission reactor to the extent of about 7 Mev per fission. The spectrum and intensity of these gamma rays must be known in order to provide a source term for any straightforward aircraft reactor shield calculation. An investigation to determine the prompt-gamma-ray spectrum resulting from thermal fission of U^{235} was initiated some time ago – it was later suspended because of the necessity of performing other experiments – and the data obtained in a preliminary experiment[1] gave a spectrum over the small energy range covered (0.5 to 2.3 Mev) that was comparable to the results reported by Smith, Fields, and Friedman[2] for Cf^{252} and by Francis and Gamble[3] for U^{235}. However, it is considered extremely important that the most careful and precise measurements possible be completed in order to enable proper account to be taken of the prompt-gamma-ray source in all future calculations of the performance of shields such as those for the complex reactor systems visualized for aircraft propulsion. Preparations, as described below, are now being made for this type of experiment.

Experimental Apparatus

As described previously,[1] the apparatus for the prompt-gamma-ray experiment consists of a spiral fission chamber viewed by the collimator of a multiple-crystal scintillation spectrometer. This type of spectrometer was chosen for its reasonably unique response characteristics. The entire assembly in its lead and lithium shield is placed upon the top of the thermal column at the Bulk Shielding Facility (BSF), as shown in Fig. 6.3.1. Gamma rays detected in the spectrometer are recorded if they are observed in time coincidence with an event in the fission chamber, within the experimental time resolution. The experimentally observed pulse spectrum, related to the desired gamma-ray spectrum by the instrument response characteristics, is measured with the aid of a multiple-channel pulse-height analyzer. All such electronic equipment is largely common to other experiments in which the multiple-crystal spectrometer is used.

A somewhat altered experimental apparatus is now being checked for possible experimental difficulties. One of the major changes has resulted in a narrowing of the usable time resolution from 0.2 μsec, as in the previous experiments,[1] as well as in another experiment,[3] to about 0.06 μsec. This improvement was attained without the use of "fast" pulse amplifiers by reducing, through the use of novel circuitry, variations in the time interval between a physical event in a detector and the appearance of the corresponding timing pulse.

Another change in the pulse-height analysis system will allow for the more rapid accumulation of data required by the experiments. This will be effected by replacing the several 20-channel pulse analyzers with a 128-channel analyzer (or 256-channel analyzer, if necessary). It has been necessary to introduce a number of rather minor circuit modifications, both to assure generally satisfactory performance of the pulse-height analyzer and to adapt it to the requirements of the specific experimental configuration. As a result, the instrument has recently been used considerably and can now be considered to perform almost within expectations. Some further investigations will be required.

Preliminary Instrument Tests

The improvement of time resolution allows for a search for delayed gamma radiation over a period after fission which could conceivably cause confusion in the experimental definition of prompt-gamma radiation if large numbers of delayed gamma rays were emitted during the same period. However, an experimental observation of the change

---

[1] F. C. Maienschein *et al.*, *Phys. Semiann. Prog. Rep. March 20, 1955*, ORNL-1879, p 57.

[2] A. B. Smith, P. R. Fields, and A. M. Friedman, *Phys. Rev.* 104, 699 (1956).

[3] J. E. Francis and R. L. Gamble, *Phys. Semiann. Prog. Rep. March 20, 1955*, ORNL-1879, p 20.

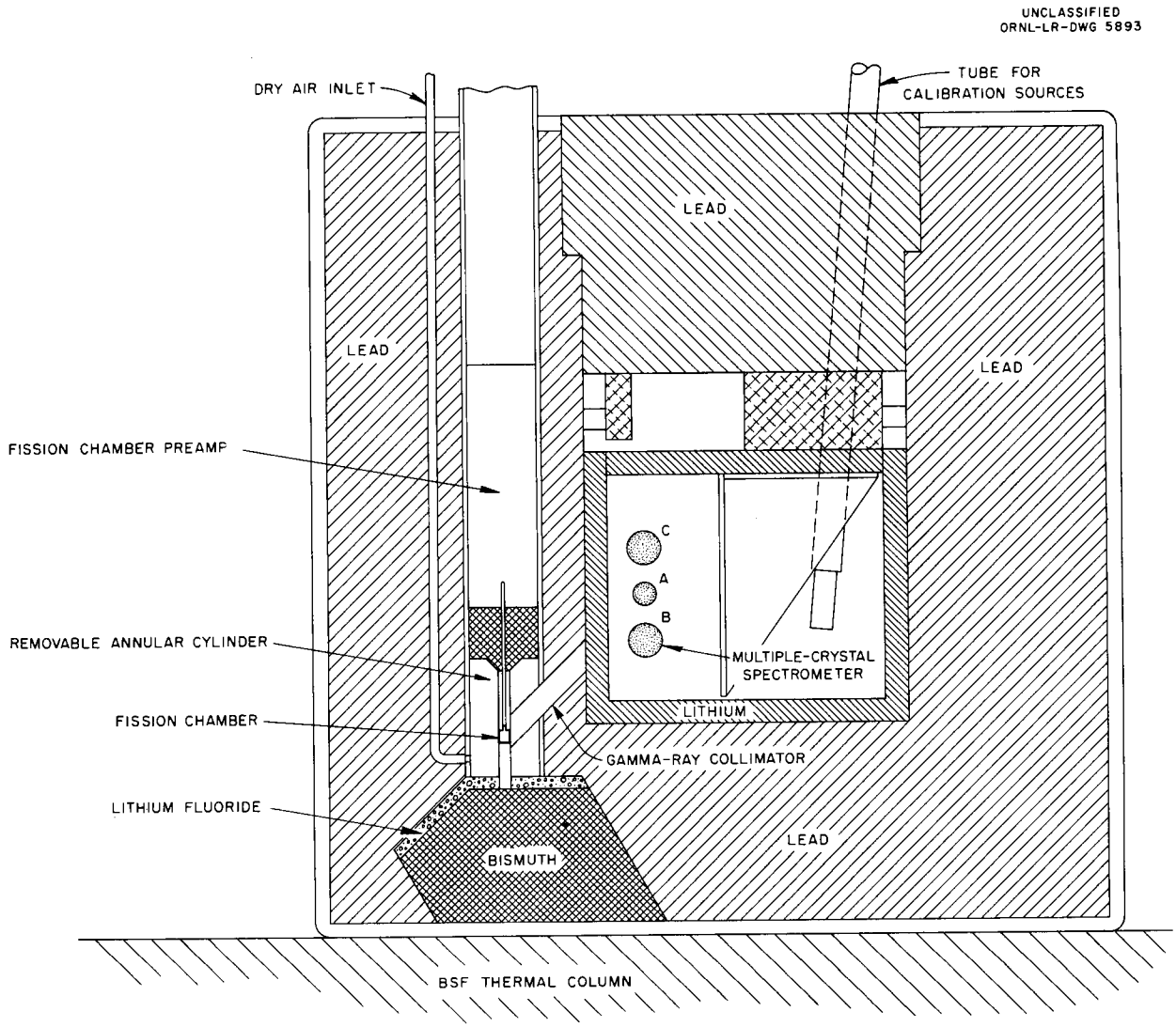

Fig. 6.3.1. Experimental Apparatus for Measurement of the Spectrum of Prompt Fission Gamma Rays.

in the apparent coincidence rate between fission events and the observation of photons in the spectrometer as a function of delays artificially introduced into one leg of the timing circuit indicated that such events do not contribute observably to the measured spectrum.

It also has been suggested that there is a danger of detecting fast prompt fission neutrons. While the thallium-activated sodium iodide scintillation detectors used are not directly sensitive to fast neutrons, such prompt neutrons can suffer inelastic scattering events in the crystal or its neighboring structure that will lead to the detection of the de-excitation gamma rays. Such gamma rays have been experimentally observed and have been correlated with the results of Day[4] for the inelastic scattering of fast neutrons in NaI. The intensity of such gamma rays seems to be concentrated at the low energies (less than 1.0 Mev), where the results of the prompt fission gamma-ray experiment are not so important for shielding purposes. The observed intensity is several times that which had been estimated.

[4]R. B. Day, *Conference on Neutron Physics by Time-of-Flight Held at Gatlinburg, Tennessee, November 1 and 2, 1956*, ORNL-2309, p 90 (June 17, 1957).

Future Work

The equipment required for the prompt fission gamma-ray spectrum experiment is largely in condition, except that the linearity of the pulse analyzer must be improved. Before the experiment begins, methods of reducing the effect of spurious fast-neutron detection upon the observed "gamma-ray" spectrum will be investigated.

ANALYSIS OF THE FISSION-PRODUCT GAMMA-RAY ENERGY SPECTRUM EXPERIMENT

W. Zobel R. W. Peelle
T. A. Love G. M. Estabrook

The data collected during the course of the experiment[5,6] to determine the gamma-ray energy spectrum and time-dependence characteristics of the decay of the fission products of U^{235} are now being analyzed in an attempt to obtain final corrected results. The required corrections involve mostly more careful analysis of the fission rates in the uranium samples observed by the spectrometers and the correction of the data for the nonuniqueness of the scintillation spectrometers.

In the experiment the nonuniqueness problem was minimized as much as possible by the use of a multiple-crystal scintillation spectrometer whose response is reasonably unique. For such instruments a large fraction of all pulses produced by a single gamma-ray energy appear approximately at the pulse height corresponding to that gamma-ray energy. (In a single-crystal spectrometer the number of pulses observed at a given pulse height and in a prescribed pulse-height interval generally includes undesired pulses corresponding to all gamma rays with energies greater than the energy of the gamma ray which it is desired to measure.) Even though the uniqueness has been maximized in the present instrument, it is important to remove from the results, as much as possible, the residual nonuniqueness in order that the corrected results will be directly interpretable. Considerable calculational efforts have been expended upon a method designed to remove almost completely the nonuniqueness effects. A complete response matrix was formed and inverted with the aid of the Oracle. These efforts failed in that the final results appear to be meaningless, but it is not presently clear whether the failure was due to a mistake in execution or to the propagation of experimental error through the adopted calculational procedure. Such error propagation may have led to errors in the corrected spectral quantities that were larger than the quantities themselves. Efforts are now under way to distinguish the cause of the failure and to develop a simpler procedure of analysis.

AFTER-SHUTDOWN GAMMA-RAY DOSE MEASUREMENTS

J. D. Kington

In order to check predictions of the gamma-ray dose emitted from a reactor after it has been shut down, a short series of integral dose measurements is planned. A preliminary experiment has already been performed, and the results are presented here because they are considered to be more reliable than other after-shutdown data previously obtained with the BSF reactor.[7] It is to be emphasized, however, that these data are still preliminary and should be disregarded when further information becomes available.

In the experiment a 900-cm^3 graphite ion chamber[8] was placed in the water surrounding the reactor on the center line approximately 63 cm from the reactor face. A completely water-reflected reactor loading consisting of fuel elements that contained fission products from previous operations was used. In two independent tests, 24 hr apart, the reactor was operated at 100 kw for 1 hr, and gamma-ray dose rate measurements were taken for approximately 14 hr after reactor shutdown. Current from the ion chamber was collected with a direct-current integrator, counted and timed with a Berkeley universal counter and timer, and printed by a Berkeley digital recorder. The results are shown in Fig. 6.3.2 with the background from previous operations subtracted. The intensity of the gamma-ray field resulted in nonlinear operation of the ion chamber. A source

[5] W. Zobel and T. A. Love, *Appl. Nuclear Phys. Ann. Prog. Rep. Sept. 10, 1956*, ORNL-2081, p 95.

[6] W. Zobel and T. A. Love, *ANP Quar. Prog. Rep. Sept. 10, 1956*, ORNL-2157, p 291.

[7] T. V. Blosser and M. K. Hullings, *Decay Gamma-Ray Dose Rate Measurement at the BSF*, ORNL CF-53-6-1, Rev. (April 12, 1955); see also E. B. Johnson and J. L. Meem, *Determination of the Power of the Bulk Shielding Reactor*, Part II, *Neutron Flux Measurements in Several Beryllium Oxide–Reflected Critical Assemblies* esp Appendix G, p 105, ORNL-1438 (April 21, 1953).

[8] L. H. Ballweg and J. L. Meem, *A Standard Gamma Ray Ionization Chamber for Shielding Measurements*, ORNL-1028 (July 9, 1951).

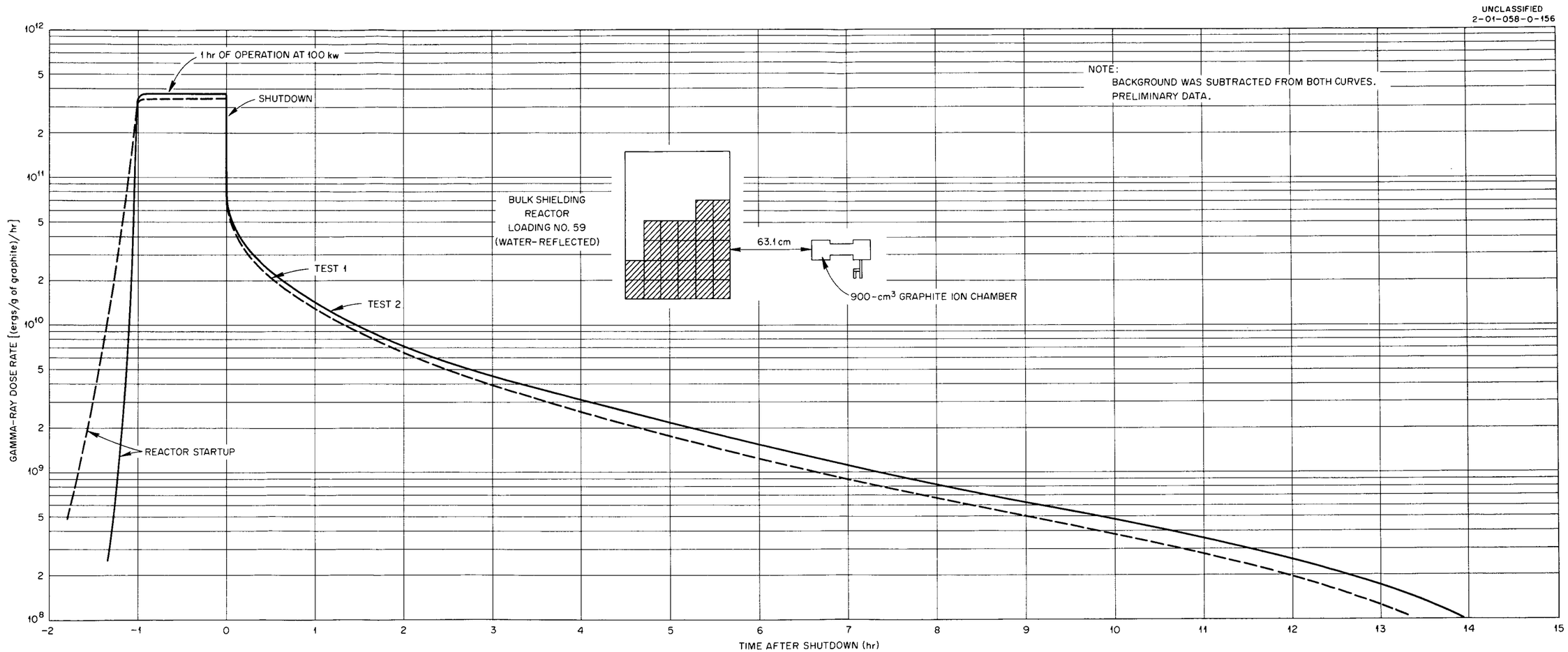

Fig. 6.3.2. Gamma-Ray Dose in the Water Surrounding the Bulk Shielding Reactor After Reactor Shutdown.

brought too near the reactor monitron caused a reactor scram, which changed the rise time in the startup of the curve for test 1.

FEASIBILITY STUDY OF A CIRCULATING-FUEL REACTOR FOR SHIELDING TESTS

J. S. Lewin[9]

A study was carried out to determine the feasibility of constructing a circulating-fuel reactor at the BSF for aircraft shield tests. Since a determination of the flux emerging from a typical reactor shield as a function of both energy and angle requires only a few kilowatts of reactor power, a power level <10 kw was assumed for the study. It was also assumed that the core volume would be 3 ft^3. Three fuel systems were considered. One was a mixture of molten fluoride salts which would most nearly reproduce the radiation spectrum of interest. This fuel system would have the disadvantages of involving high temperatures and requiring a complex heat supply system to keep the fuel mixture fluid. Another fuel considered was UF_6 dissolved in C_8F_{16}. The disadvantages associated with this system are the instability of the fuel under irradiation and the extreme chemical activity of UF_6 gas. The system UO_2SO_4 dissolved in D_2O appeared to be the fuel mixture which would be the most feasible, although the nuclear characteristics of a heavy-water solution are considerably different from those of the fluoride salts proposed for the circulating-fuel reactor. Also there is a danger of D_2O_2 being formed in the solution. Extensive nuclear calculations would be required to demonstrate the degree of nuclear approximation available from a D_2O system. Consideration would also have to be given to the use of a D_2O reflector with the addition of a neutron-capture solute to mock up the capture gamma rays from the beryllium reflector of the circulating-fuel reactor.

PROGRAM FOR SHIELDING MEASUREMENTS AT THE ART

G. T. Chapman

The installations which will be necessary to make gamma-ray spectroscopic, neutron spectroscopic, and gamma-ray and neutron dose measurements at various points within the ART shield during reactor operation were described in a previous report.[10] Recently, studies have been made of the preoperation schedule that must be followed for calibration and efficiency measurements of the instruments. These measurements will be made by placing gamma-ray sources of various known energies at the geometric point in space that will coincide with the point of interest on the reactor shield and by observing the resulting source spectra through each of the 50-ft-long collimator tubes. In order that these measurements may be made with confidence, the components of each tube must be in place and the measurements must be made before and after the "bullnose" caps are placed on the reactor end of the spectrometer tubes. In order to conform with the engineering test schedule on the pressure shell, this work must be completed by December 1, 1957. Consequently, it is anticipated that the work on fabricating the spectrometer tube components will begin on July 1, 1957, and the actual calibrations at the site will be started as soon thereafter as possible.

TOTAL ABSORPTION GAMMA-RAY SPECTROMETER

G. T. Chapman T. A. Love

It is anticipated that the detector for gamma-ray spectroscopy measurements at the ART and at the Bulk Shielding Facility will consist of one large "total absorption" thallium-activated sodium iodide crystal. Since these large crystals are not commonly in use, the characteristics of one such crystal are being investigated at the BSF. The crystal (Figs. 6.3.3 and 6.3.4) is approximately a 9-in.-dia cone with one truncated end. Collimated beams of gamma rays of various energies are introduced at different locations on the crystal surface, and the resulting shapes of the pulse-height spectra are observed.

Preliminary experiments have been performed to determine the collimator geometry that would have a minimum effect on the final data. The collimator finally chosen consisted of a ¼-in.-dia by 10-in.-long hole in a lead block. It is believed, though it has not been definitely proved, that this collimator reduces any exterior effects to a minimum. Some time has also been spent observing the effects of phototube gain misalignment, since the scintillations in the

[9] On assignment from The Glenn L. Martin Co.

[10] G. T. Chapman, *ANP Quar. Prog. Rep. Dec. 31, 1956*, ORNL-2221, p 348–351.

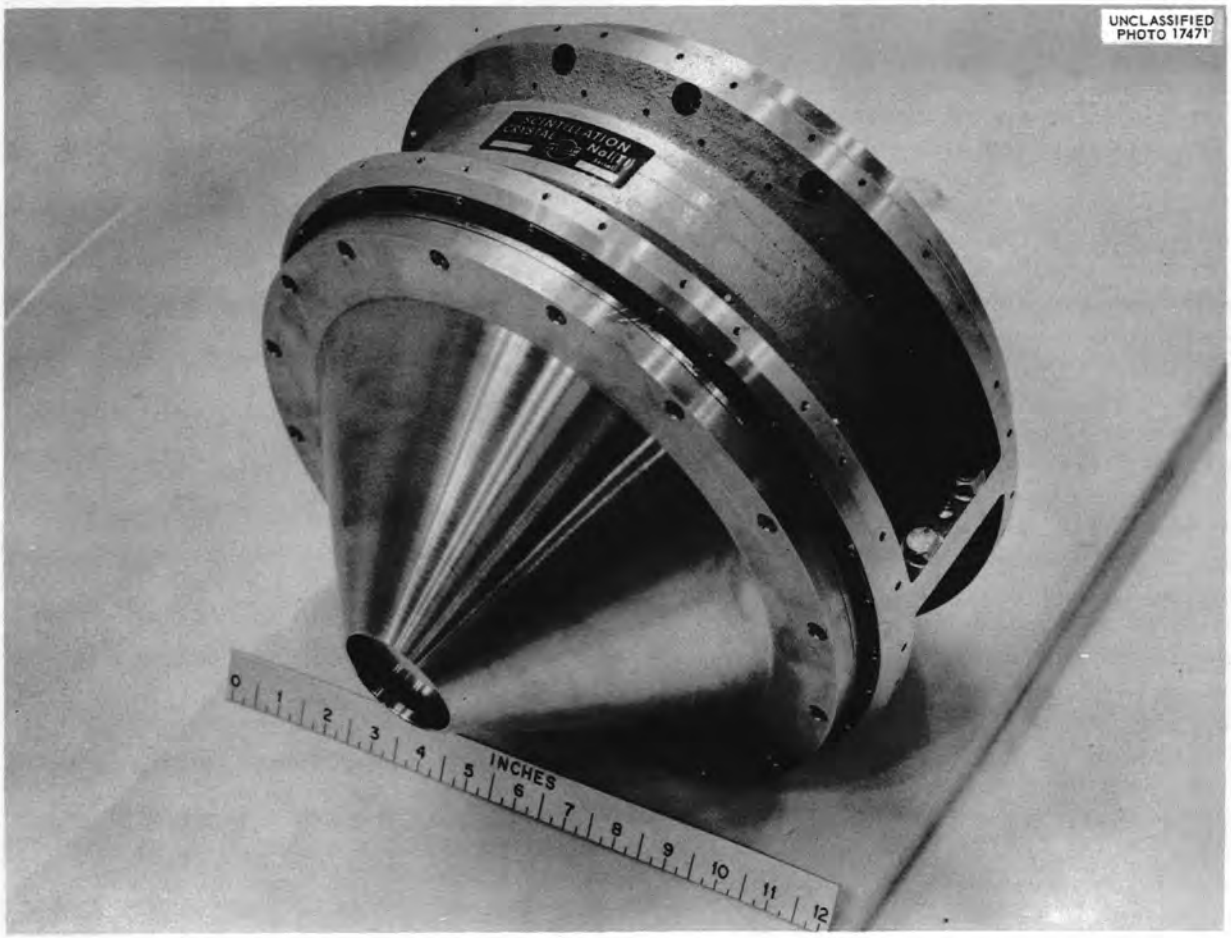

Fig. 6.3.3. Photograph of the 9-in.-dia Aluminum-Canned Thallium-Activated Sodium Iodide Crystal. (Note: The gamma rays will normally enter the crystal through the small truncated end of the cone.)

crystal will be observed with multiple phototube arrangements. The present arrangement consists of three 5-in.-dia phototubes operated in series, with the voltage supplied through a voltage divider from a common supply. The arrangement is such that the voltage is monitored at the power supply and at each phototube independently. There is apparently a real effect with tube gain misalignment. This is demonstrated by comparing Figs. 6.3.5 and 6.3.6. Figure 6.3.5 shows the photopeak for Cs^{137} (0.662 Mev) that was obtained with different gains of the three tubes; that is, the voltage was adjusted on each individual phototube so that the resulting photopeaks were separated by about ten channels when the phototubes were run individually with a common amplifier gain. The measured resolution (percentage full width at half-peak maximum) was found to be about 16%. Figure 6.3.6 shows the same photopeak with the phototube voltages adjusted so that they showed a common gain. In this case the measured resolution was found to be 12.5%. By applying a Gaussian distribution of the form

$$Y(E) = Y(E_0) \exp \left[-\frac{2.772}{R^2} \left(\frac{E - E_0}{E_0} \right)^2 \right]$$

with a crude fit to the upper edge of the photopeak, it is possible to obtain some idea of the distortion for each situation. This effect is also shown in Figs. 6.3.5 and 6.3.6.

Considerable data have been taken with the 2.76-Mev gamma ray from Na^{24}. These data were taken

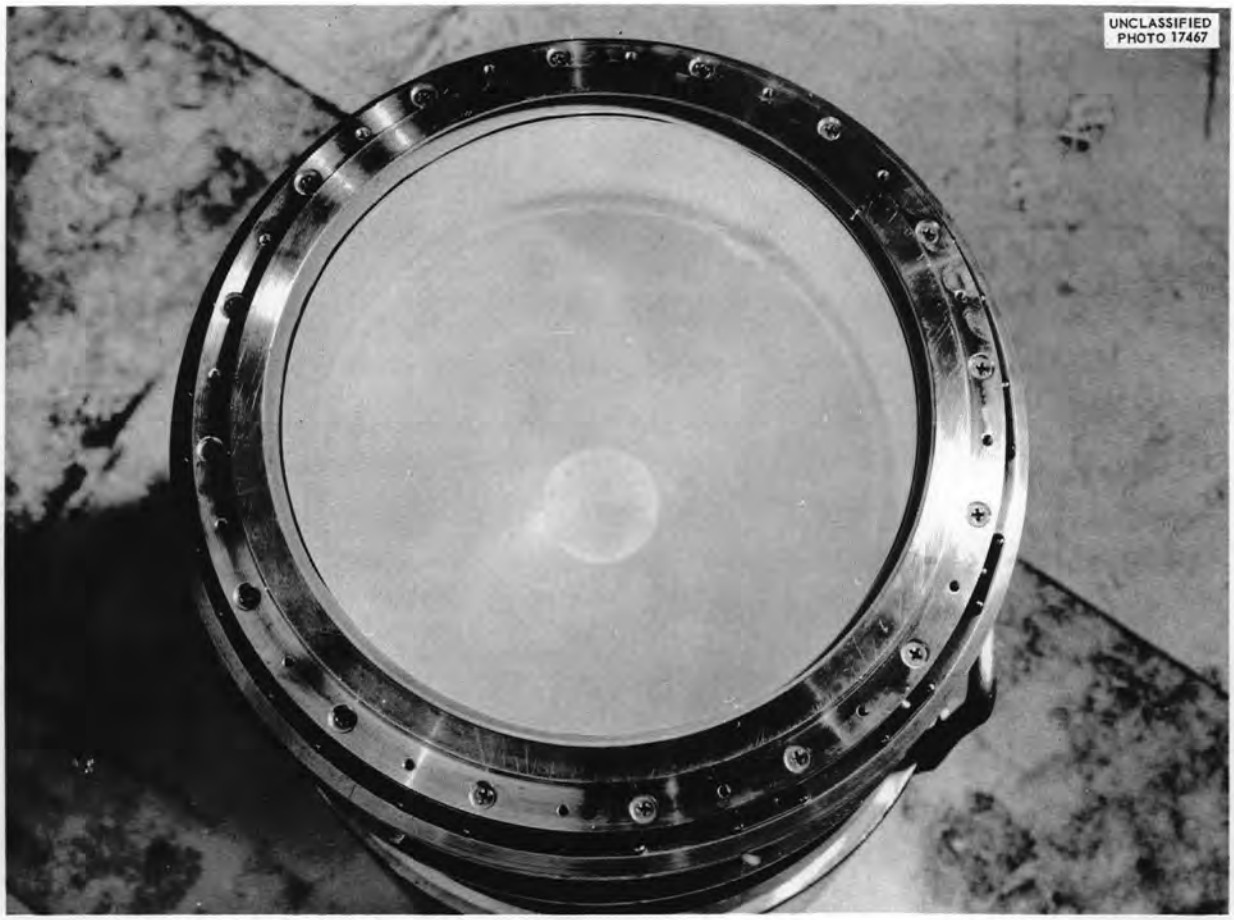

Fig. 6.3.4. View of the Large End of the Crystal Shown in Fig. 6.3.3.

in the form of traverses along the side of the crystal. In general it has been observed that the resolution changes from about 18% to about 8% as the gamma rays are collimated into the side of the crystal at successive locations away from the 2-in.-dia truncation of the cone (see Fig. 6.3.3). Figure 6.3.7 shows the peak obtained with the 2.76-Mev gamma-ray beam going into the small truncated end of the crystal, and Fig. 6.3.8 shows the same peak with the beam entering perpendicular to the side of the cone and 5 in. from the end. It has not been proved whether this effect is or is not due entirely to a discontinuity in the crystal. The data are being studied at present in an attempt to see whether the observed distortion may be due to Compton back-scattering. If it is, the distortion may be eliminated by drilling a well in the crystal to minimize such escapes.

THE BSF MODEL IV GAMMA-RAY SPECTROMETER HOUSING AND POSITIONER

R. W. Peelle T. A. Love
F. C. Maienschein

It has been recognized for some time that integral shielding measurements which measure only the flux or dose and, therefore, do not give information concerning angular distributions or energy spectra are, in principle, not sufficiently detailed for the design of complex shields and are of interest only when such integral quantities are directly desired. If tissue dose is measured with a complete mockup of the shield system, a nonoptimum design may be accomplished with dose measurements alone, even though the processes taking place within the shield cannot be determined. By taking extremely detailed integral measurements, it has been possible

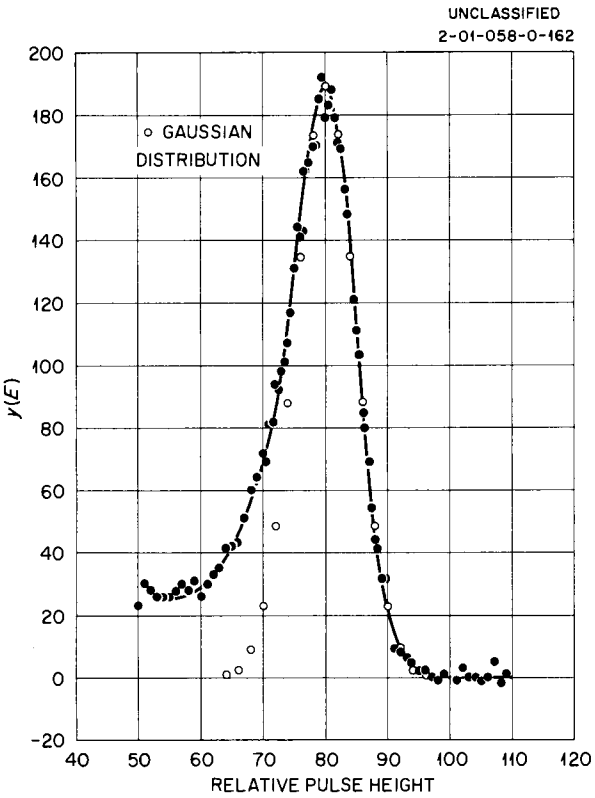

Fig. 6.3.5. Response of the 9-in.-dia Crystal to 0.662-Mev Cs^{137} Gamma Rays with the Phototube Gains Misaligned (Resolution = 16.1%).

to infer enough information to arrive at reasonable shield designs, even for divided shields. However, it is felt that, for ANP shield design, detailed energy and angular spectra for the region of the reactor shield will be required, at least for certain test cases. For example, calculations of air scattering for a divided shield depend upon the details of the radiation leaving the reactor shield. The calculations are not presently adequate to predict such energy and angle spectra, and if they were it would still be necessary to subject the calculated results to a detailed experimental check for at least a few shield configurations.

Such detailed information is needed for both gamma rays and neutrons. In order to obtain the gamma-ray spectra at the BSF it will be necessary to position a gamma-ray spectrometer collimator within 1 cm of any desired point in the pool at an angle known to within a fraction of a degree. Since a large number of spectra will be required, it is also important that the measuring system be simple and reliable.

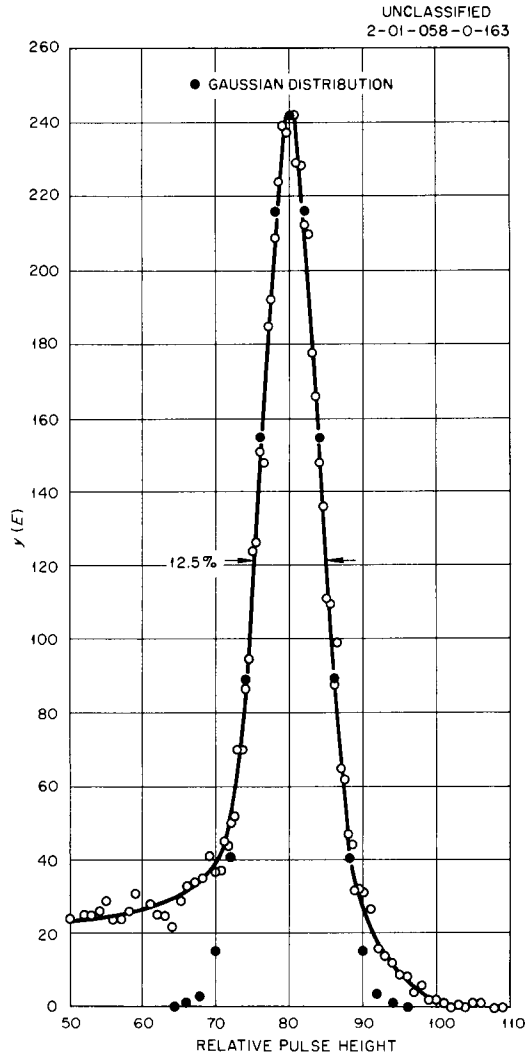

Fig. 6.3.6. Response of the 9-in.-dia Crystal to 0.662-Mev Cs^{137} Gamma Rays with the Phototube Gains Aligned (Resolution = 12.5%).

The BSF model IV gamma-ray spectrometer, which consists of a scintillation detector and an appropriate housing and collimator, will be used for the measurements. The entire assembly, which will weigh in excess of 15 tons, must be supported by a specially designed positioner (see below). The design of the shield (that is, the housing) and the collimator arrangement is illustrated by Fig. 6.3.9. This design is based on the use of a "total absorption" sodium iodide scintillation spectrometer, which consists essentially of a 9-in.-dia right cylinder of the scintillation material. Such a spectrometer would combine high efficiency, reasonable uniqueness of response, and simplicity

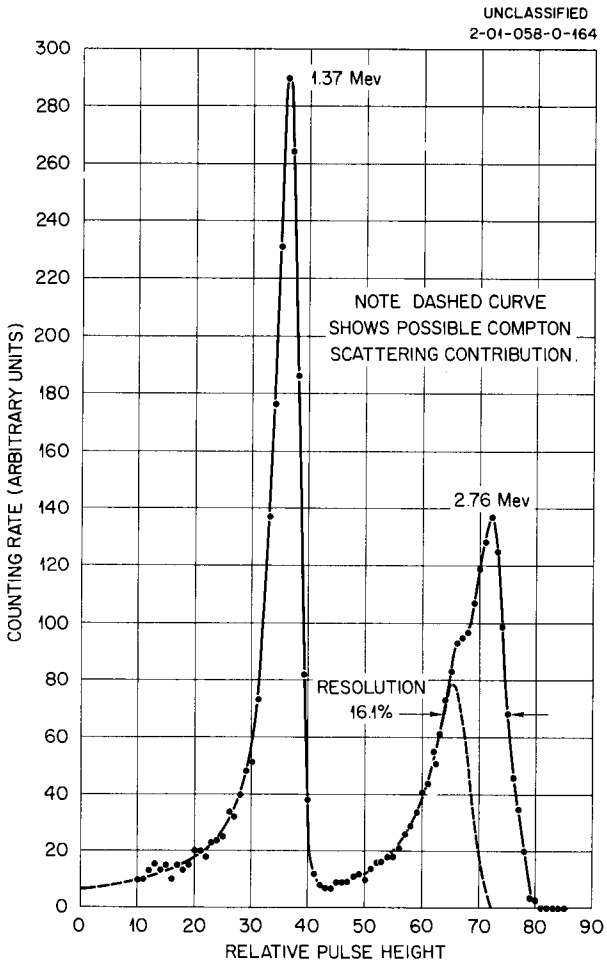

Fig. 6.3.7. Response of the 9-in.-dia Crystal to 2.76- and 1.37-Mev Na^{24} Gamma Rays Collimated into the Truncated End of the Crystal.

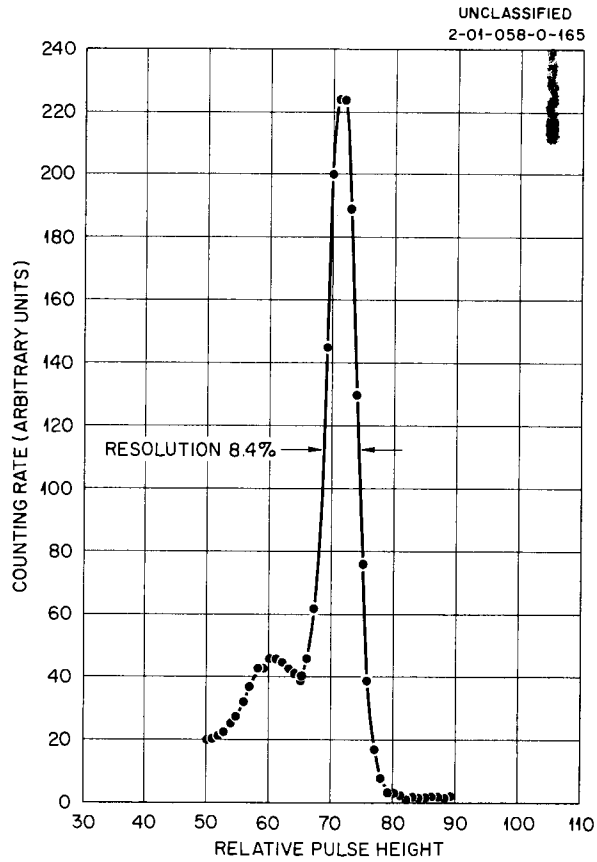

Fig. 6.3.8. Response of the 9-in.-dia Crystal to 2.76-Mev Na^{24} Gamma Rays Collimated into the Crystal 5 in. from the Truncated End.

of operation (see section above, this chapter, on "Total Absorption Gamma-Ray Spectrometer"). If such a spectrometer does not prove to be feasible, a modified and improved form of the multiple-crystal scintillation spectrometer will be utilized.

The spectrometer collimator (Fig. 6.3.9) will consist of two rings several inches apart. The rings will probably be constructed of high-density tungsten alloy, which will be helpful in assuring that the solid angle viewed by the unit will not be a strong function of photon energy. These rings will be interchangeable. In order that background measurements and spectrometer calibrations can be effected efficiently, the collimator will be intersected with a lead cylinder that will be rotatable about an axis perpendicular to the collimator direction. Rotation of this lead cylinder will provide at least three usable positions. In one position a hole through the lead cylinder (perpendicular to the cylinder axis) will be aligned with the holes through the tungsten rings so that a straight-through hole from the spectrometer to the edge of the shield will be effected. In another position a solid lead section will plug the collimator for background measurements. A third position will place a source adjacent to the inner tungsten ring for calibrations.

When a large sodium iodide crystal is used in the vicinity of a reactor source, considerable care must be taken to avoid background effects caused by neutron radiative captures in the materials of the crystal. This problem will be alleviated by making it more probable for the neutrons to be captured in lithium, since such captures do not lead to radiative transitions. The lithium will be provided in the shield, which will be cast from a

[redacted]
ORNL-LR-DWG 21559

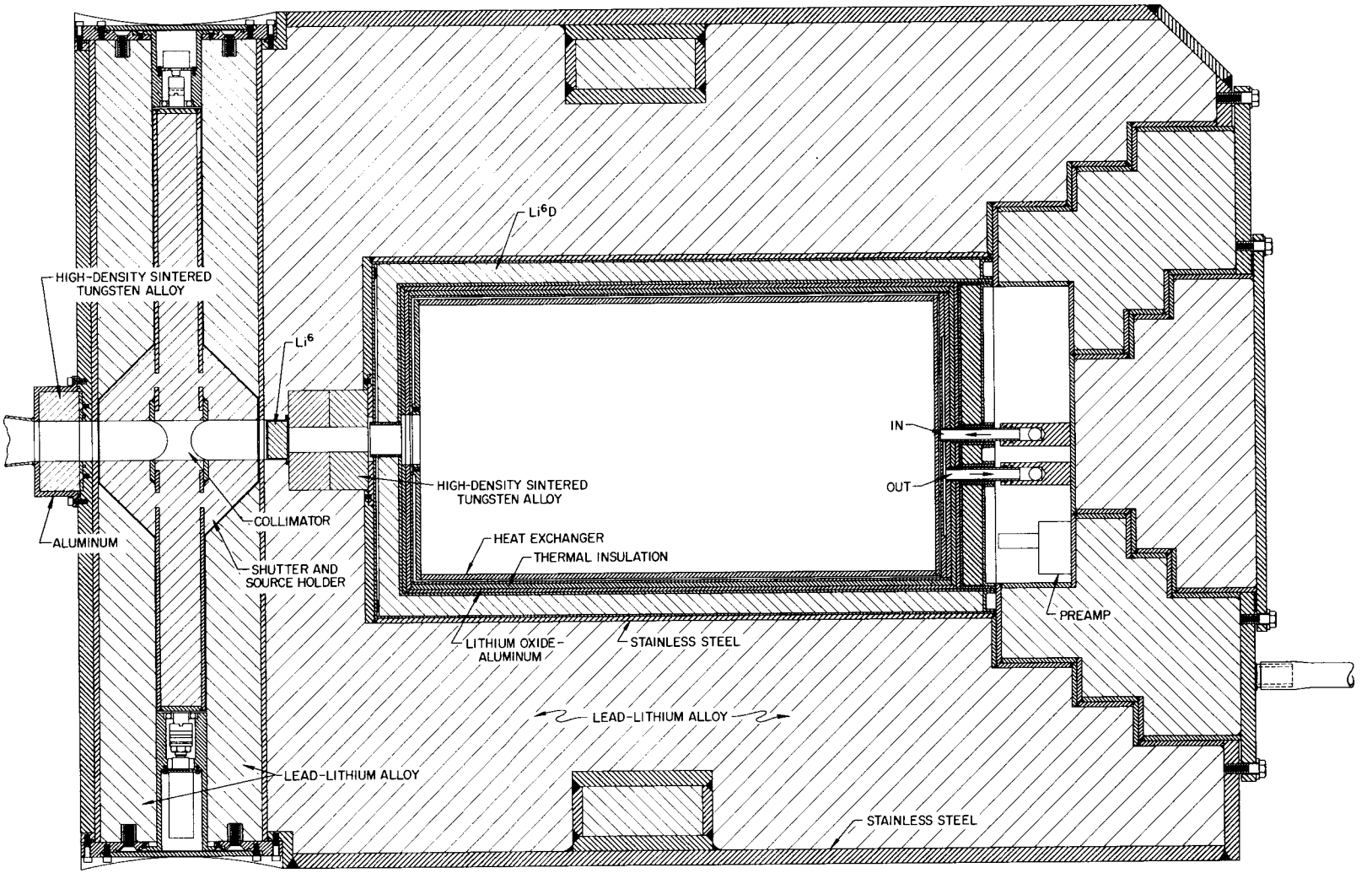

Fig. 6.3.9. Proposed Housing and Collimator Arrangement for the BSF Model IV Gamma-Ray Spectrometer.

lead-lithium alloy. Within the cavity of the lead shield there will be a stainless-steel-canned container of Li^6D, which will further reduce activation by resonance neutrons, and possibly a final thin layer of lithium oxide cermet. These measures, while costly, are considered to be necessary on the basis of previous unsatisfactory experience with improperly shielded spectrometers. The precautions will be most necessary, of course, when the spectrometer is being operated in a region of relatively high neutron flux. Figure 6.3.10 shows a photograph of the can which contains the lithium deuteride neutron shield. The design of the model IV spectrometer shield is complete except for design details which may be affected by studies now being made of the feasibility of the use of the lithium-lead alloy.

A sketch of the proposed spectrometer positioner is presented in Fig. 6.3.11. The vertical I-beams shown are building supports to which rails have been attached at a 10-ft elevation for the support of cross rails which, in turn, support the spectrometer through a long telescoping vertical column. The spectrometer shield is mounted on trunnions at the base of these columns and can be rotated or tilted. The shield may be placed at any desired position in the pool or lifted clear of the pool wall for maintenance of the internal apparatus or for calibration tests. The positioner will be controlled from a console located on the carriage directly above the spectrometer, and sensing devices will be available for measuring the detector position at all times.

Fig. 6.3.10. Stainless Steel Container for Li^6D Neutron Shield for the BSF Model IV Gamma-Ray Spectrometer. (Confidential with caption)

A LOW-SENSITIVITY GAMMA-RAY ION CHAMBER FOR RADIATION DAMAGE STUDIES

J. D. Kington

A 4-cm^3 ion chamber (Fig. 6.3.12) for measuring gamma-ray energy deposition in graphite in a high-intensity field of the type that would be encountered in a radiation damage testing facility was tested and calibrated. The experiment described here was conducted in an attempt to ascertain the degree of collection of ionization as a function of radiation field and chamber voltage. For these tests the BSF reactor was operated at 200 kw. (Measurements will be made at 1 Mw as soon as practical.) Figure 6.3.13 shows the saturation curves for the 4-cm^3 ion chamber, as well as those for three other ion chambers, including the new isotropic-response 50-cm^3 spherical ion chamber. The currents were measured with (1) a Beckman micromicroammeter, (2) an electrometer and galvanometer, and/or (3) a current chopper feeding a Berkeley universal timer and printer.

The detector response with the high-voltage lead disconnected was found to be less than 1% of the chamber reading. In order to measure the center of detection, a new apparatus for locating the source with respect to the ion chamber was constructed. Chamber and source positions are now reproducible to within ±0.1 cm. Plots of measurements taken with this ion chamber agree, in shape, with those of earlier measurements[11] for distances out to 240 cm from the reactor.

[11] F. C. Maienschein *et al.*, *Attenuation by Water of Radiations from a Swimming Pool Type Reactor*, ORNL-1891 (Sept. 7, 1955).

UNCLASSIFIED
ORNL-LR-DWG 21560

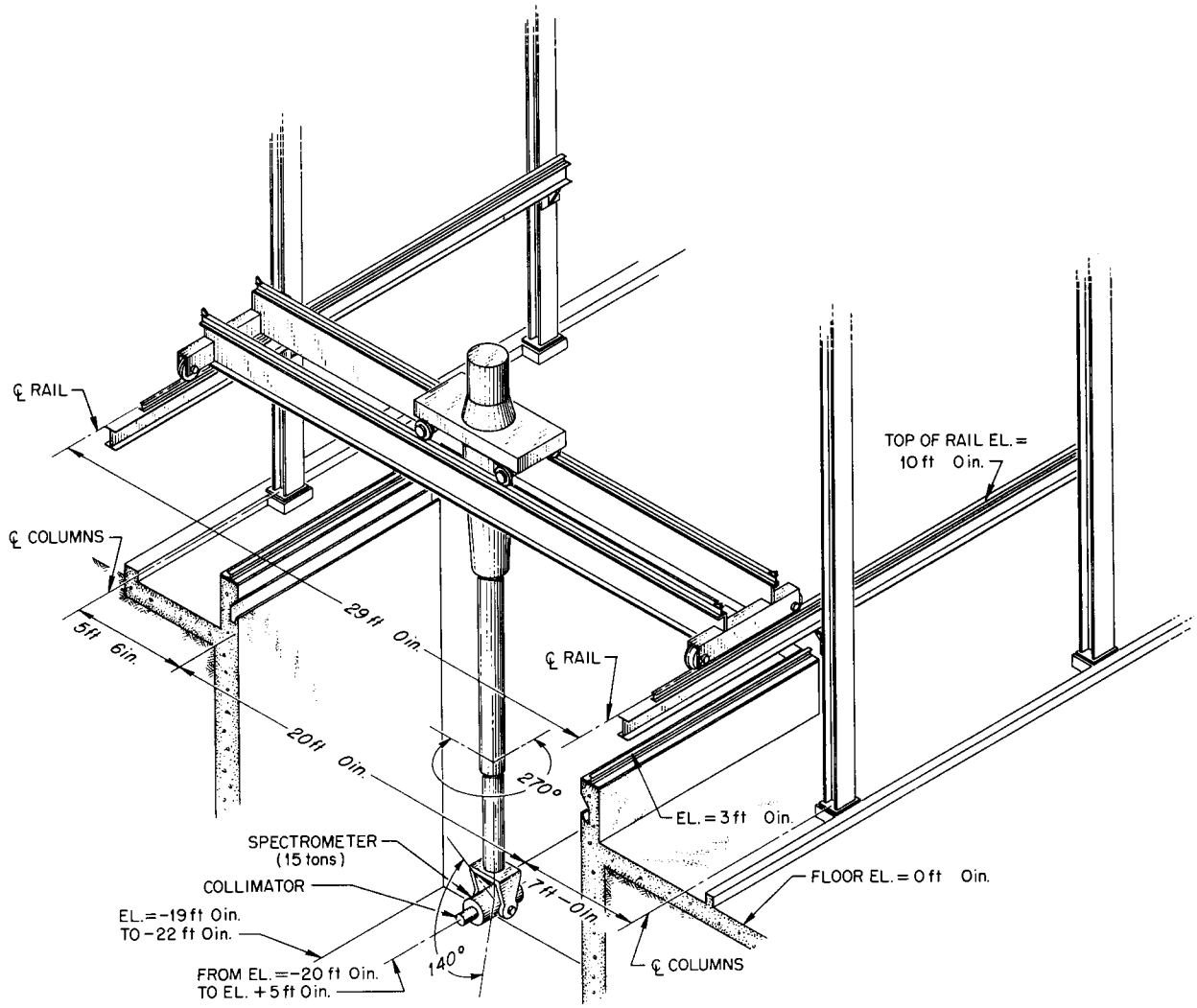

Fig. 6.3.11. Proposed Design for the BSF Gamma-Ray Spectrometer Positioner.

UNCLASSIFIED
2-01-058-0-166

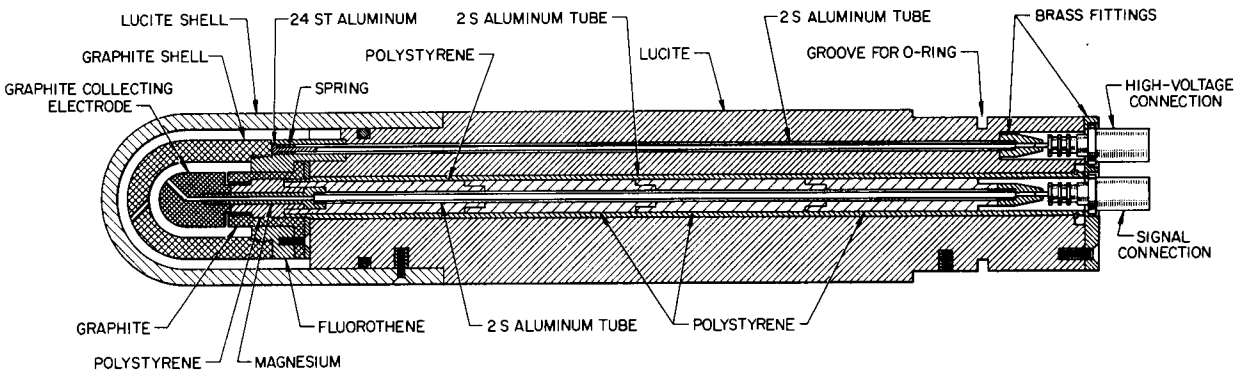

Fig. 6.3.12. A Low-Sensitivity Gamma-Ray Ion Chamber.

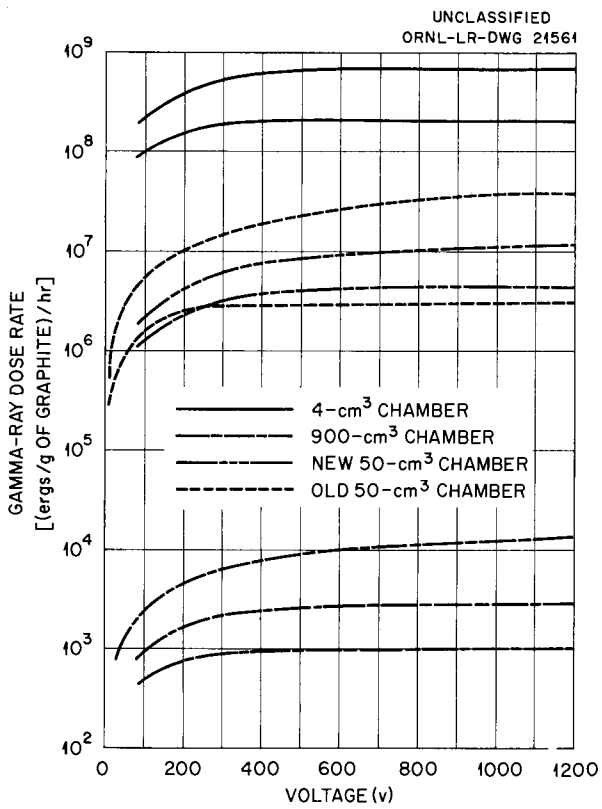

Fig. 6.3.13. Saturation Properties of Several Gamma-Ray Ion Chambers.

PULSED-NEUTRON METHOD FOR THE DETERMINATION OF NEUTRON DIFFUSION PARAMETERS IN BERYLLIUM

E. G. Silver G. deSaussure

Most reactors proposed for aircraft propulsion utilize beryllium as the reflector or moderator. One of the important parameters needed in order to accurately perform calculations for such reactors is the neutron diffusion coefficient of beryllium. An experiment is now being planned to determine this parameter in beryllium at elevated temperatures. The experiment will apply the so-called "pulsed-neutron method," which was first described by von Dardel.[12] The method consists of releasing a short burst of fast neutrons into a block, cylinder, or sphere of the material under investigation and then observing the decay with time of the thermal-neutron population. By an analysis of this time-decay rate for several different sizes of blocks of the material, the value of the diffusion coefficient as a function of temperature can be determined. Less material will be required in this method of obtaining the diffusion coefficient than is required for the standard steady-state method. Further, at elevated temperatures, it would be difficult to position sources and detectors inside the material as required by the steady-state method.

The temperature variation of the diffusion coefficient in beryllium at elevated temperatures is not computable because various crystal changes take place in beryllium in this temperature range which are not well understood. In order to clarify some discrepancies between results obtained by various experimenters who have used this method heretofore and in order to acquire some familiarity with the technique, an initial experiment will be performed with cubes of graphite. Graphite is a particularly suitable material for study since it also is expected to exhibit marked crystal modifications.

Since the time for decay of thermal neutrons in blocks of the size to be used in this experiment is of the order of micro- or milliseconds, it is necessary to have experimental apparatus of some complexity in order to measure the time behavior of the neutrons accurately. An 18-channel variable-frequency-controlled time analyzer has been designed and built for this purpose and is in the final stages of testing.

The short bursts of neutrons will be produced by pulsing an ion accelerator, which will be used with either deuterons or tritons on a target of deuterium, to produce *d-d* or *d-t* neutrons. A 300-kv accelerator has been designed and is in the process of construction. It is anticipated that the accelerator, except for the power supply, will be completed by June 1, 1957. However, since the power supply will not be available before 1958, the initial phases of the experiment will be performed at the ORNL High-Voltage Laboratory (Bldg. 5500) with an accelerator available there.

[12] G. F. von Dardel, "The Interaction of Neutrons with Matter Studied with a Pulsed Neutron Source," *Kgl. Tek. Högskol. Hændl.* (*Trans. Roy. Inst. Technol., Stockholm*) NR75, 185 (1954).

A UO_2–STAINLESS STEEL SHIELD TEST REACTOR FOR THE BSF

A calculation published previously[13] demonstrated the expected hardening of the gamma-ray spectrum from a reactor core containing a stainless steel component as compared with that of the present BSF reactor containing aluminum. The resulting higher energy spectrum would correspond more closely to the leakage spectrum of the ART or to the spectrum of any other proposed aircraft reactor employing structural materials of the Fe-Ni-Co system. Since it is primarily the gamma-ray spectrum which varies from reactor to reactor, rather than the neutron spectrum, a reactor containing a UO_2–stainless steel core would provide an appreciably better source of reactor radiations for aircraft shielding studies than does the present BSF reactor. It has therefore been proposed that such a reactor be constructed for the BSF within the next year. This reactor would not replace the present reactor, which has a uranium-aluminum core, but would be interchangeable with it.

There are several other advantages to this new type of core. With the proposed near-cubical design, a reactor radiation source of minimum size would be attained which would permit maximum flexibility in wrapping shields around the reactor core. Further, if the planned control system, which will utilize "plate-type" control devices, is nearly as effective as preliminary results indicate, major perturbations introduced by the control devices would be markedly reduced and the more nearly symmetrical leakage flux needed in order to accurately analyze shield tests would be obtained. The reduced perturbation could be achieved even though the larger absorption cross section for the UO_2–stainless steel core would require more absorber than the present core for equal control. In addition, installation of this core will test the corrosion resistance of the stainless steel in reactor fuel elements. It is well known that the aluminum cladding of the present fuel elements is penetrated by corrosion pits within two to three years in process water, although the life of the elements is expected to be extended considerably in the demineralized water now being used at the BSF. For many research reactors, the useful portion of the fuel-element reactivity lifetime could probably be extended to much longer periods with a more durable structural material such as stainless steel.

The mechanical features of the proposed reactor and, in particular, the control devices are described below. The criticality calculations that have been performed to date are presented, and a summary is given of the results from a preliminary experiment performed to evaluate the reactivity control to be achieved with the proposed plate-type control devices.

Description of the Reactor

J. S. Lewin[14]

The basic loading of the stainless steel reactor will consist of 25 MTR-type fuel elements in a cubical 5- by 5-element lattice with a core volume of 3300 in.^{3}. The elements will be clad in AISI type 347 stainless steel with end plates and end boxes of the same material. Figure 6.3.14 shows the cross section and over-all dimensions of the fuel elements, grid plate, and control mechanism.

Fuel Elements and Grid Plate. – The fuel elements will be approximately 3 in. square in cross section and may be rotated ±90 deg without affecting adjacent elements. The control plates and the four special fuel elements associated with them (see below) will maintain the same cross section. Each fuel element will consist of 20 fuel plates, each containing a fuel section 15 in. high by 2.60 in. wide by 0.020 in. thick. The stainless steel cladding over the fuel will be 0.005 in. thick. End boxes of the fuel elements will be minimized in size to reduce the amount of parasitic capture near the core.

The material selected for the grid plate is the precipitation-hardening stainless steel 17-7 PH. Since this steel can be hardened to an R_C of 40, a grid plate design which will permit reduction of the grid plate thickness to 0.85 in. will be used. The grid plate will be ground to a surface flat to within 0.006 in. The fuel-element end boxes will have ground pedestal surfaces that will rest on the grid plate and $2\frac{3}{8}$-in.-dia shanks that will be used only for positioning the fuel elements in the lattice. Three strips pressed into and projecting above the surface of the grid plate will prevent rotation of the fuel elements about the vertical

[13] G. deSaussure, *ANP Quar. Prog. Rep. Dec. 31, 1956*, ORNL-2221, p 343.

[14] On assignment from The Glenn L. Martin Co.

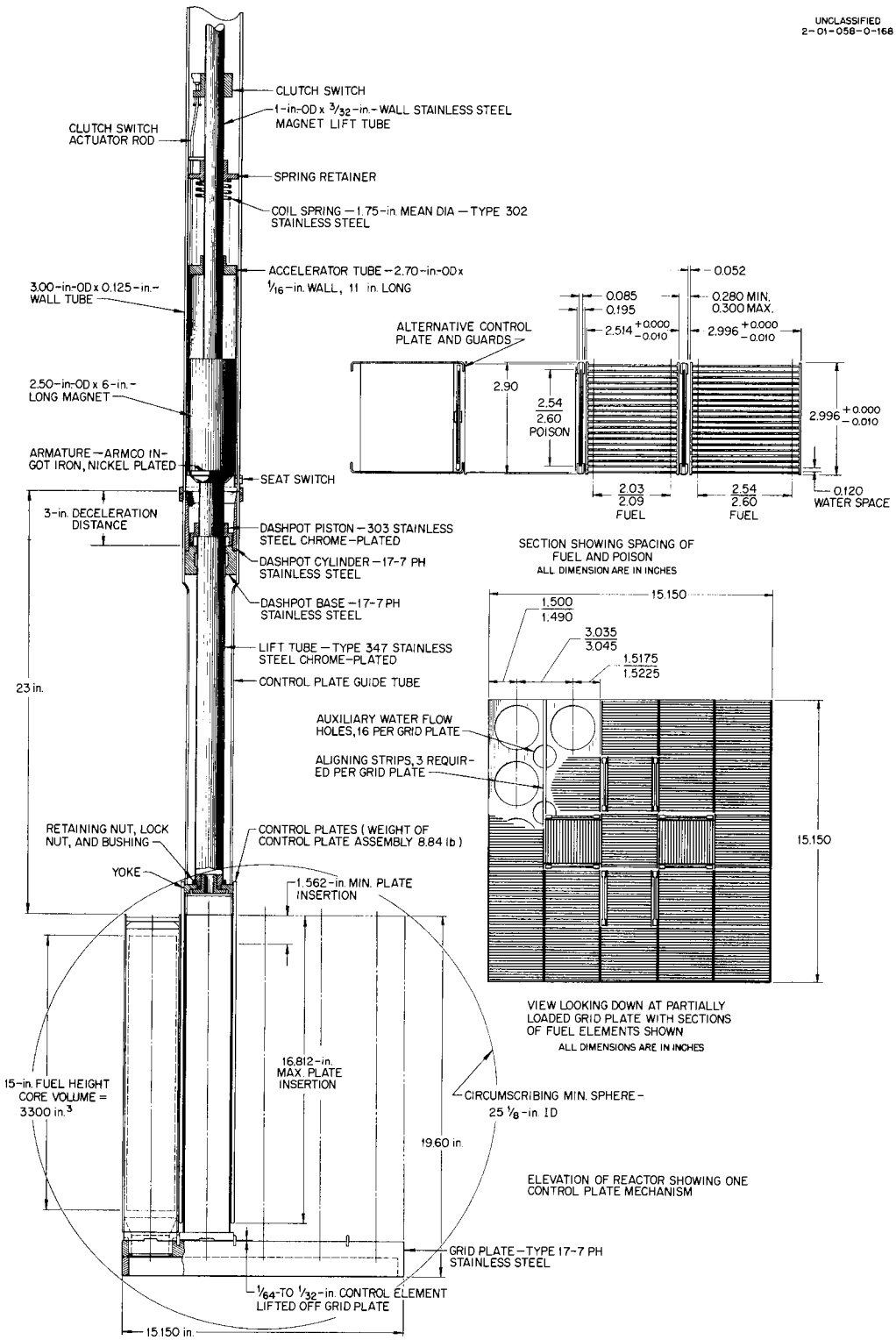

Fig. 6.3.14. Fuel-Element Arrangement and Control System for Proposed BSF UO_2–Stainless Steel Reactor.

axis. The grid plate will be stiffened by a 1-in.-thick frame to limit the deflection slope to a maximum of 0.00023 in./in.

Four fuel elements will be modified to receive the control plates, the widths being decreased to 2.514 in. across the end plates. This is equivalent to a loss of 3.7 fuel plates distributed equally between two sides of the fuel element, or 18.5% of the fuel. The resultant water gap that will exist between the modified fuel element and an adjacent fuel element when a control plate is withdrawn will be 0.280 to 0.300 in. The upper ends of the modified fuel element will be fitted with stainless steel adapters that will join the fuel element to the control-plate guide tube.

Control Plates. – The control plates and their lifting mechanism are shown in Fig. 6.3.14. The plates will be rolled sandwiches of type 347 stainless steel faces around a core of boron dispersed in iron; each plate will contain the equivalent of about 4.5 g of B^{10}. The control plates will be paired, so that four lifting mechanisms will be required for eight plates. The drive motor will be the coaxial drive unit now used on the aluminum-clad core of the BSF reactor, but it will be equipped with a thrust bearing for push as well as lift capability.

In a reactor scram, each control plate assembly will receive an initial downward acceleration of about 8 *g* which will decrease to about ½ *g* in 4½ in. This acceleration will be supplied by a coil spring and accelerator tube. Thus the drive motor will have to exert a thrust sufficient to fully compress the accelerator spring and allow the magnet to engage the armature. During this compression stroke the 20-ft-long magnet lift tube will be subjected to buckling stresses, and therefore it will be constructed of a 1-in.-OD stainless steel tube with 3/32-in.-thick walls. Once the magnet has engaged the armature, the stress in the magnet lift tube will become tensile and localized between the magnet and the spring retainer fitting 9½ in. above the magnet. The total weight of the control plate assembly will be 8.8 lb, and the weight of the spring and accelerator tube will be 2.7 lb. The total force supported by the magnet, including the 82-lb spring compression force, thus will be 93.5 lb. The buckling stress margin of safety will be +70% since a 20-ft-long tube will buckle at 138 lb. Should additional strength be required, the tube can be redesigned easily.

Calculations of the plate drop time from the fully withdrawn position were made for an initial acceleration of 6.5 *g*, assuming a dynamic water drag coefficient of 1.4 on 2½ projected areas of 2.65 in.^{2} each. (The effects of the distances between the piston, the control plates, and the armature and their respective areas were estimated to be equivalent to 2½ projected areas.) The results indicate that the net time to drop 12 in. will be 0.141 sec. This does not include magnet release time. A magnet for this reactor is being developed that is to exert a minimum 100-lb force on the armature, and the release time may be as low as 10 msec. A reduction in drop time of 50% over that of the present gravity-accelerated rods appears to be possible.

After the initial 12 in. of drop, deceleration will begin in a hydraulic dashpot in which water will be squeezed out around the piston and piston rod. Calculations of the motion during deceleration were made in which the shape of the dashpot body was varied and various coefficients of discharge through the two orifices were assumed. The dashpot body was designed as a compromise between ease of machining and the attainment of the least shock, as indicated by the calculations. The force of deceleration will be absorbed as tension in the magnet guide tube, since the control element assembly will be shimmed at the drive motor so that it will be supported at the top and will not rest on the grid plate.

Possible binding of the control plates was investigated. The space allowed for the control plates was established on the basis of fabrication tolerances and thermal expansion. If all fabrication tolerances were cumulatively consumed in the unfavorable direction, the remaining space between control plate and adjacent fuel element would not be closed up until the temperature of the metal rose to 830°F. An alternative control plate design, also shown in Fig. 6.3.14, is under consideration. In this design, channel section guards have been added at the ends of the control plate and the stiffener strips have been relocated from the ends of the control plate to the center.

It is recognized that with the first arrangement, wear of rubbing surfaces may, in time, increase the possible shifting of the relative position of the control plates and the fuel elements. An investigation of apparent coefficients of friction under water has been started. Initial results show that

smoothly finished surfaces are undesirable under even light unit pressure, since they tend to squeeze out the water between them and create a vacuum. One striated surface rubbing against a smooth surface tends to maintain a lubricating water film which exhibits an apparent coefficient of friction of 0.02 to 0.03, regardless of the materials involved.

A full-size test assembly of the control plate configuration has been fabricated and will be tested in the near future. The tests will provide data on the magnet, the motion of the control plates, distortion tendencies, and wear. Unfavorable conditions of distortion and forces will be imposed on the control plates and adjacent elements. The decision on adopting the alternative control plate will be based on results of this test.

Heat Transfer Calculations

J. S. Lewin

Preliminary heat transfer calculations were made by a method of successive approximations of the average water density in the central fuel element, as follows:

(1) $$dQ_z = q_z A\, dz \text{ (Btu/hr)} ,$$

(2) $$Q_z = xC_p(T_z - T_0) \text{ (Btu/hr)} ,$$

(3) $$x = A_w v_z \rho_z \text{ (lb/hr)} ,$$

(4) $$v_z = \left[\sqrt{2\left(\frac{\rho_0 - \bar{\rho}_z}{\bar{\rho}_z}\right) gz}\right] 3600 \text{ (in./hr)} ,$$

where

Q_z = total heat transferred to water in length z of fuel elements, Btu/hr,

q_z = heat generation rate at any point z in central fuel element, Btu/hr·in.^{3},

x = mass water flow (lb/hr),

z = dimension along length of fuel element, in.,

T_z = mean water temperature at point z, °F,

T_0 = water temperature in pool, °F,

v_z = average velocity of water flow over area A at point z, in./hr,

A = gross cross section of fuel element, in.^{2},

A_w = cross section available for water flow, in.^{2},

ρ_z = water density at point z, corresponding to temperature T_z, lb/in.^{3},

$\bar{\rho}_z$ = average water density in length z, lb/in.^{3},

ρ_0 = density of surrounding pool water, lb/in.^{3},

g = acceleration of gravity, in./sec^2,

C_p = heat capacity, Btu/lb·°F.

A simple cosine distribution of flux was assumed, with a peak-to-average flux ratio of 2.6. Based on this assumption

(5) $$q_z = \frac{2.60\,P}{3300} \sin\left(\frac{\pi z}{15}\right) \text{ (Btu/hr·in.}^3\text{)} ,$$

where P is the reactor thermal power level, Btu/hr.

The method used was to find Q_z by use of Eqs. 1 and 5. Then, x was plotted as a function of $(T_z - T_0)$. A value for $(T_z - T_0)$ was then assumed and $\bar{\rho}_z$ was obtained from a curve of ρ vs T. By using this $\bar{\rho}_z$, v_z was found from Eq. 4, after which x was found from Eq. 3. This x, substituted back into Eq. 2 should yield the originally assumed $(T_z - T_0)$. If it did not, a new $(T_z - T_0)$ was assumed and the process was repeated until assumed and resultant temperature differences checked.

The temperature of the fuel plate surface was then found from

(6) $$T_w = \frac{Q_z}{ha} + \bar{T}_z ,$$

where

T_w = fuel plate wall temperature at point z, °F,

h = average heat transfer coefficient over length z, Btu/hr·°F·ft^2,

a = surface area available for heat transfer in length z, ft^2,

T_z = average fluid temperature over length z, °F.

With 20 fuel plates per element, the plate surface temperature, T_w, in the central fuel element was found to reach 239°F, the boiling point for water under a head of 20 ft, at a reactor power of about 700 kw. The effective heat transfer coefficient h was 140 Btu/hr·°F·ft^2. At this same power level, the average water temperature rise in passing through the fuel element was 62°F. Thus the stainless steel reactor would be limited in power level to a few hundred kilowatts. Based on past

experience with the aluminum core, it is not anticipated that such a power level limitation would present any difficulties whatsoever for the performance of shielding experiments.

An identical calculation for the present BSF aluminum-clad reactor for loading 33 was compared with measured temperatures of the water. Agreement was obtained that was well within experimental accuracy. The measured wall temperatures, however, indicate that a heat transfer coefficient of 140 Btu/hr·°F·ft^2 is conservative.

Reactivity Calculations

E. G. Silver

A series of preliminary reactivity calculations were carried out to determine the feasibility of the stainless steel core for the BSF. All the calculations were performed on the UNIVAC with the use of the so-called Eyewash code, which is a 30-group, multiregion, one-dimensional, spherical-geometry code. The code has 30-group nuclear parameters as part of its tape library, and these are used as input parameters. The necessary specifications are the magnitude of Δr, the radial grid spacing, the number of regions and the number of grid spacing widths of each region, the nuclear density or volume fraction of each component of each region, and the self-shielding factor in each region. Type 302 stainless steel is one of the materials available with this code, and, since it is very similar from the nuclear standpoint to the type 304 stainless steel planned for use in the core, it was used in these calculations. The Eyewash code uses the Goertzel-Selengut approximation for neutron slowing down in a hydrogeneous moderator but considers no binding effects on diffusion lengths at low energy. Calculations previously performed with this code for the aluminum BSF reactor core with one control rod[15] indicate that this method should be capable of giving results to within a few per cent in critical mass.

The first calculations were for a 15-in.-high, 5 by 5 element, UO_2–stainless steel core configuration containing control rods of the shape and design used in the BSF reactor. For this purpose 4 of the 25 fuel elements were assumed to have space for control rods in the positions shown in Fig. 6.3.15*a*. This geometry was approximated in two ways, as shown in Fig. 6.3.15*b*. In model 1

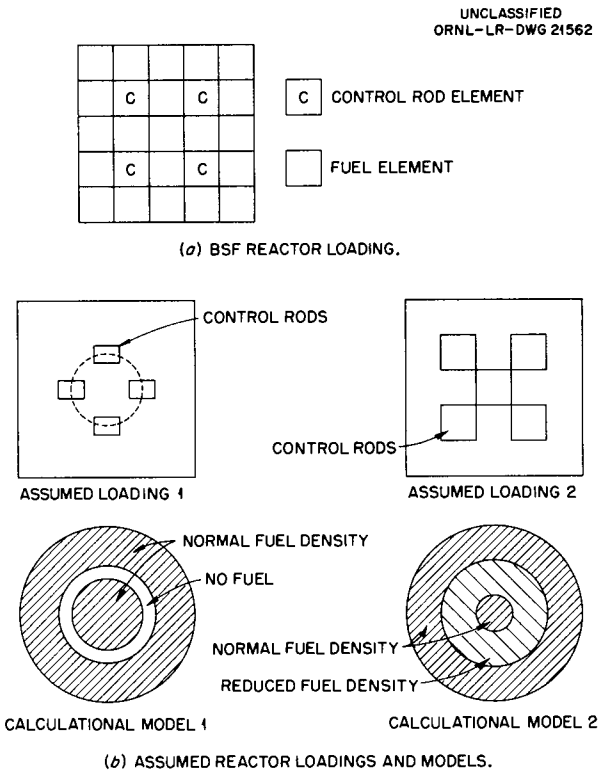

Fig. 6.3.15. Models Used for Calculations of the Critical Mass of a UO_2–Stainless Steel Core Containing a 5 by 5 Element Loading and Four Control Rods.

the actual volume of the control rod wells and guide plates was taken to be a nonfueled region with a volume calculated to have the same fraction of the sphere as it does in the actual reactor. In model 2 the four control rod elements in their entirety were taken as a separate region with a reduced fuel density. The outer sphere dimensions were calculated by the equation

$$R = \frac{1}{\left[\left(\frac{1}{a+2\delta}\right)^2 + \left(\frac{1}{b+2\delta}\right)^2 + \left(\frac{1}{c+2\delta}\right)^2\right]^{1/2}}\ \delta,$$

where

R = radius of the sphere used in the calculation,

a, b, c = outside dimensions of the fuel-element array,

δ = reflector savings, given by $(D_c/D_r)L_r$,

[15] E. G. Silver, *Appl. Nuclear Phys. Ann. Prog. Rep. Sept. 10, 1956*, ORNL-2081, p 47.

D_c, D_r = thermal diffusion coefficients in the core and reflector, respectively,

L_r = thermal diffusion length in the reflector.

Each fuel element for the first set of calculations was assumed to consist of 20 fuel plates, each having a 25-mil-thick fuel section clad with 5-mil-thick stainless steel on each side. The side plates were considered to be 50 mils thick. It became apparent that a fuel section of this thickness was not necessary; therefore, a second set of calculations was performed for a fuel section reduced to a 20-mil thickness. In all cases it was considered to consist of powder-sintered UO_2 and stainless steel, with a maximum UO_2 content of 25 wt % and a density which was 92% of the theoretical density. This composition permitted a maximum fuel loading of 12.7 kg of U^{235} in the case of the 25-mil-thick fuel section and 10.2 kg in the case of the 20-mil-thick fuel section. A small correction had to be made in the calculation for extra silicon in type 304 stainless steel.

The calculations based on model 1 resulted in a critical mass of 6.6 kg of U^{235}. For model 2 the mass was 6.3 kg of U^{235}. This corresponds to a fuel-plate section containing about 17 wt % of UO_2. Figure 6.3.16 is a plot of the calculated neutron source strength and thermal-neutron flux on the basis of model 1; the extremely sharp rise near the edge of the void may be seen. This rise is more pronounced than it would be in an aluminum reactor because of the higher absorption cross section of the stainless steel core. In such a core the fuel plates adjacent to the control rod well would be the limiting ones in terms of heat transfer. Since the void would be narrower if plate-type control devices were used and consequently this flux peaking effect would be diminished, calculations were next performed utilizing configurations with control plates rather than rods.

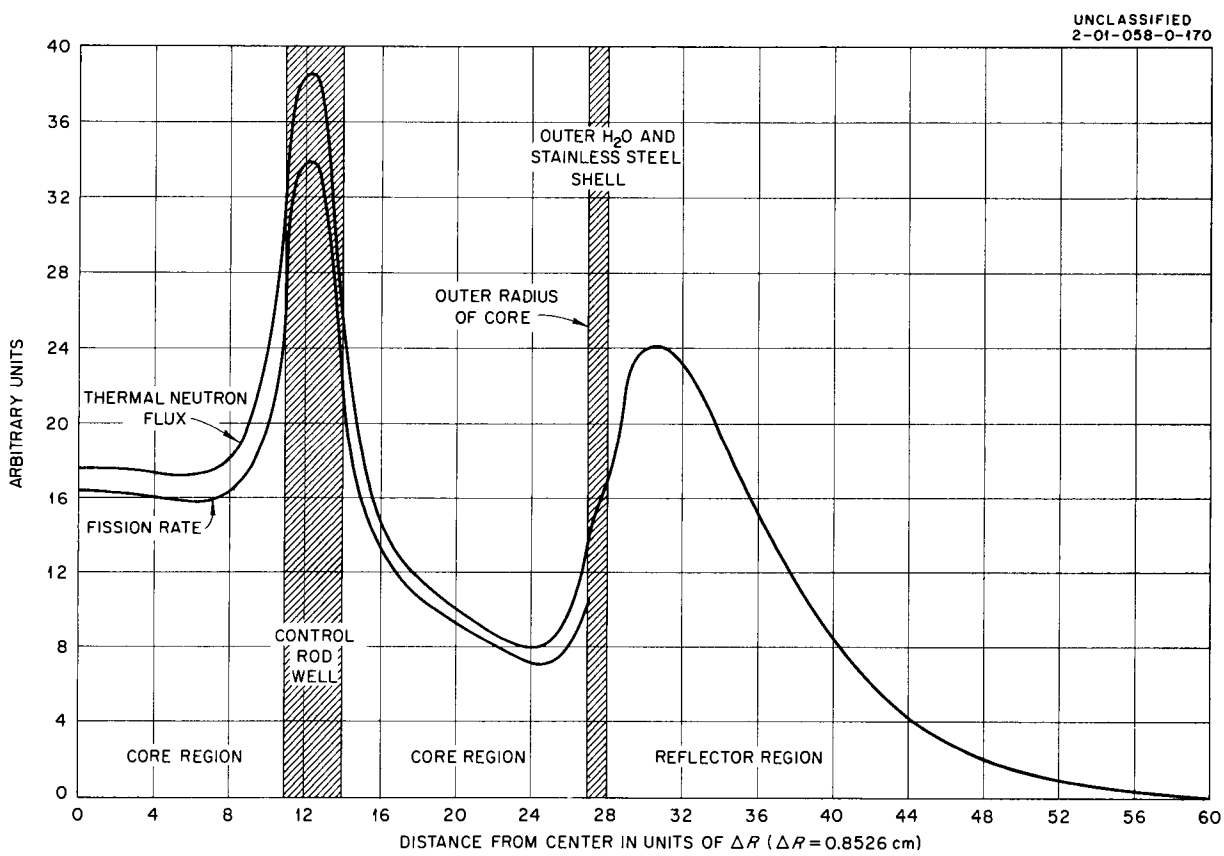

Fig. 6.3.16. Calculated Thermal-Neutron Flux and Fission Rate in a UO_2–Stainless Steel Core Containing a 5 by 5 Element Loading and Four Control Rods (Model 1).

Calculations were first performed for a 15-in.-high, 5- by 5-element configuration containing eight control plates. The control plates were assumed to be substituted in pairs for fuel plates in four different elements. A homogeneous core was assumed, and the calculated critical mass was 5.9 kg of U^{235} or about 14.0 wt % UO_2.

Since the fuel density in these calculations was much less than the maximum density available, it was decided to perform calculations for a smaller core, a 12-in.-high, 4- by 4-element array. The calculated critical mass was greater than 12 kg. This core also proved to have a very epithermal spectrum, as shown in Fig. 6.3.17, in which the fraction of fission caused by neutrons above a given energy for this core is compared with that for the 25-element core. Corresponding information for an aluminum core is also presented. Calculations with fuel elements containing 35 wt % UO_2 were also attempted, but they overflowed on the computing machine because of too large a ratio of cross sections in adjacent regions.

Calculations were also performed for a configuration containing only four control plates in elements especially constructed for them. These control plates were assumed to be just outside the element side plates and therefore perpendicular to the fuel plates. In the first calculation the fuel section of each fuel plate was assumed to be of variable thickness and to contain 25 wt % UO_2. A 5-mil-thick stainless steel cladding on the plates was also assumed. The calculated critical mass fell outside the range of calculation, but an extrapolation indicated a critical mass of about 4.0 kg of U^{235}, which would correspond to a fuel section thickness of 7.4 mils in each fuel plate. This thickness was too little in that it would make the total plate thickness only 17.4 mils. The calculation was therefore repeated for a 20-mil fuel section thickness and variable UO_2 enrichment. The critical mass was determined to be about 5.6 kg.

A more recent design that utilizes a square lattice unlike that of the BSF reactor is now being considered, and calculations for this configuration will be undertaken in the near future.

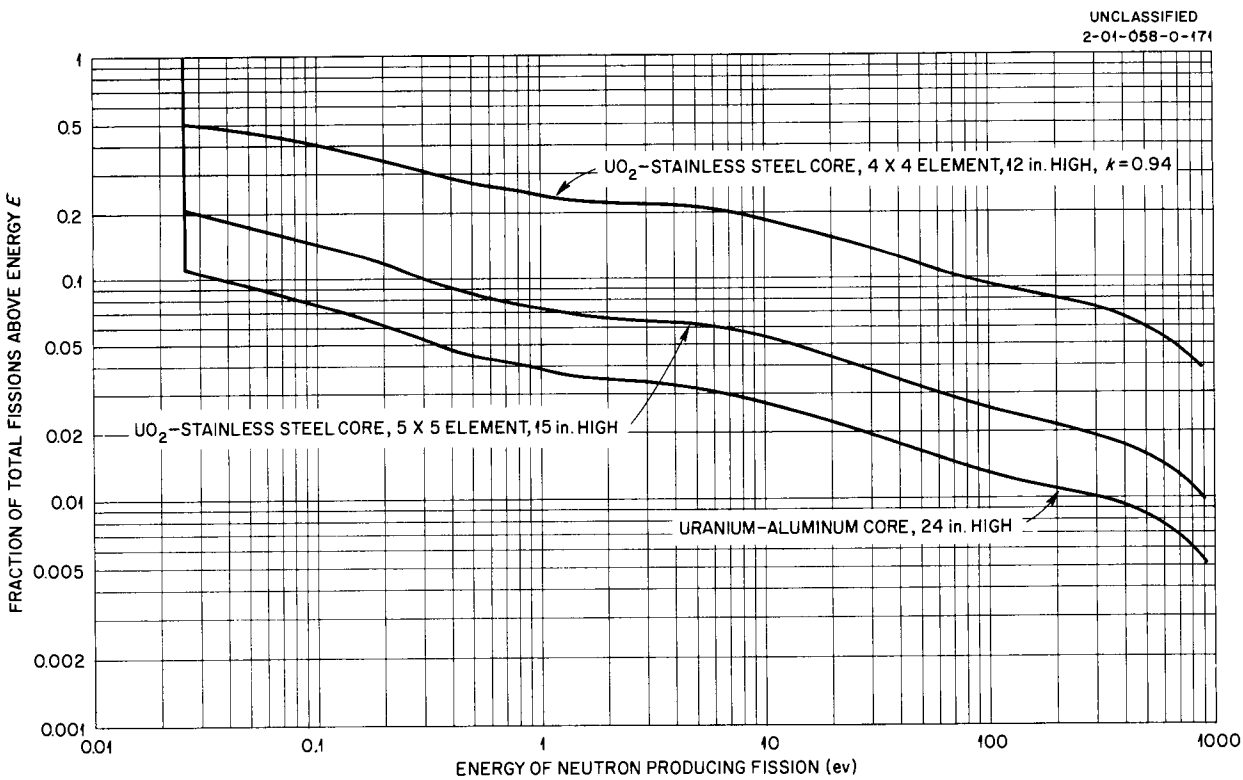

Fig. 6.3.17. Calculated Fractions of Fissions Occurring Above Energy E in Various Reactor Configurations as a Function of E.

Control Plate Experiments

K. M. Henry J. D. Kington
E. B. Johnson A. B. Reynolds

Experimental tests to determine the effectiveness of single plates of absorber were performed with the aluminum core of the BSF reactor since no stainless steel reactor is available. Extrapolation from the aluminum to the stainless steel core is not straightforward, but it is more reliable than a direct calculation for the stainless steel core.

The reactivity effects of the test control plates were determined in two positions in the reactor core. The loading used consisted of 30 elements in a 5 by 6 array, as shown in Fig. 6.3.18. This loading had a critical mass of about 3.5 kg of U^{235} and contained 1.5% excess reactivity. The effect of the test plates located near the edge of the core was measured by inserting each test plate in place of the seventh fuel plate from the concave side of element B-151 in lattice position 4. The effect of the test plates located near the center of the core was determined by moving element B-151 to the center lattice position (position 25).

Five stainless steel plates containing only type 304L stainless steel were tested. Plate thicknesses ranged from 0.032 to 0.125 in., as shown in Table 6.3.1. The variation in thickness of each plate was less than ±0.001 in.

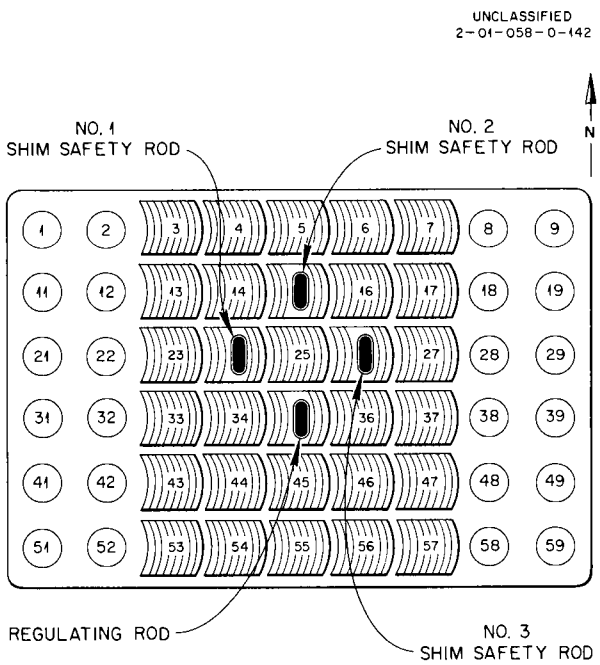

Fig. 6.3.18. Bulk Shielding Reactor Loading No. 57.

Ten boron-containing plates were also tested. These plates consisted of a core of boron carbide powder compacted with aluminum powder and clad with 2S aluminum by hot rolling. In the five plates containing 1, 2, 4, 8, and 16 g of natural boron, respectively, about 20 g of inert Al_2O_3 was added to the core in order to increase the density of the compacted mixtures to enough above that of aluminum to be able to see the outline of the cores under a radiograph while preparing the plates. The approximate dimensions (after rolling) of the boron-containing cores in each plate are given in Table 6.3.2.

Table 6.3.1. Effect of Type 304L Stainless Steel Plates on Reactivity in BSF Reactor Loading 57

Thickness of Plate (in.)	Reactivity Change (% $\Delta k/k$)	
	Lattice Position 4 (Near Edge)	Lattice Position 25 (Near Center)
0.032	−0.051	−0.152
0.049	−0.079	−0.223
0.077	−0.119	−0.33
0.122	−0.166	−0.46
0.125	−0.160	−0.46

The total thickness of each of the five plates containing 1 to 16 g of boron was approximately 50 mils. The plates containing 20 and 50 g of boron were each approximately 110 mils thick. The effect of inserting pure aluminum plates of the same thicknesses was also determined for comparison with the effect of the boron-containing plates.

Reactivity measurements were made by comparing the regulating rod positions before and after each test plate was inserted into the core with the regulating rod calibration curve shown in Fig. 6.3.19. The regulating rod was calibrated by use of the inhour equation, which relates the change in the reactivity ($\Delta k/k$) to the stable reactor period.

The results of the reactivity measurements for the stainless steel plates in positions both near the edge and near the center of the core are given in Table 6.3.1. The effect on the reactivity of

Table 6.3.2. Effect of Boron-Containing Plates on Reactivity in BSF Reactor Loading 57

Weight of Boron (g)	Plate Thickness (in.)	Length of Plate Core (in.)	Width of Plate Core (in.)	Reactivity Change (% $\Delta k/k$)			
				Lattice Position 4 (Near Edge)		Lattice Position 25 (Near Center)	
				Effect of Boron and Aluminum	Effect of Boron Only	Effect of Boron and Aluminum	Effect of Boron Only
0	0.052			−0.010	0	−0.022	0
1	0.053	22.6	~2.44	−0.189	−0.179	−0.52	−0.494
2	0.053	22.6	~2.44	−0.276	−0.266	−0.76	−0.74
4	0.054	22.6	~2.44	−0.381	−0.37	−1.11	−1.09
8	0.053	22.6	~2.44	−0.501	−0.49	−1.47	−1.45
16	0.052	22.6	~2.44	−0.595	−0.58		
0	0.114			−0.022	0		
20	0.114	21.4	2.19	−0.60	−0.57		
50	0.118	21.2	2.25	−0.67	−0.65		
50	0.118	21.2	2.25	−0.69	−0.67		

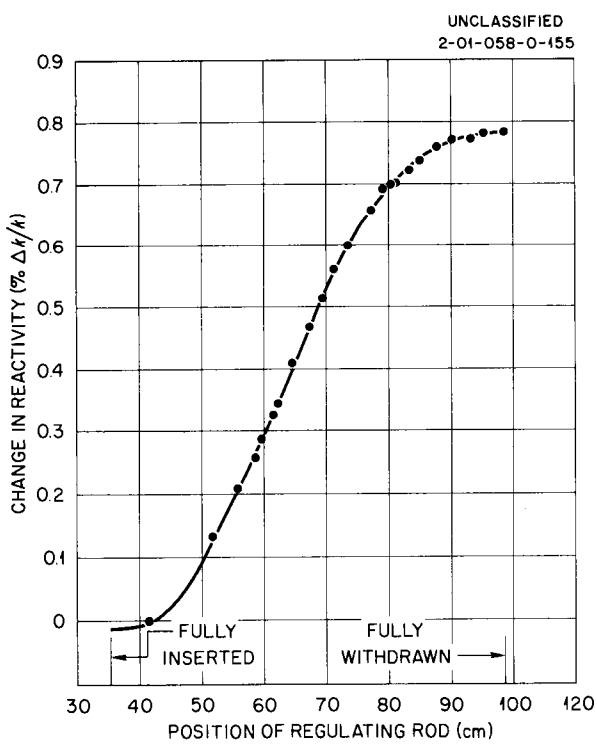

Fig. 6.3.19. Calibration Curve of 87-mil Stainless Steel Regulating Rod in BSR Loading No. 57.

inserting stainless steel plates in the core as a function of the plate thickness is plotted in Fig. 6.3.20 for both positions. Also plotted in this figure are the changes in reactivity that result when a fuel plate is replaced by a stainless steel plate.

The results of the reactivity measurements for the natural-boron-containing aluminum plates in positions both near the edge and near the center of the core are presented in Table 6.3.2. For each position, values are given for the effect of the boron plus the aluminum and for the effect of the boron alone. In Fig. 6.3.21 the change in the reactivity caused by the boron alone is plotted for both positions as a function of the weight of boron in the plates. Insufficient excess reactivity was present in the loading to determine the effect of any plates containing more than 8 g of boron when located near the center position of the core. Additional experiments are planned with a different fuel element loading having greater excess reactivity in order to extend the data to higher boron concentrations.

Although the boron plates containing more than 8 g of boron could not be tested at the center of the core, it is noted that the ratio between the

reactivity measurements for the 1- to 8-g boron plates in the two positions lies between 2.76 and 3.01. Furthermore, the ratio of the results for the stainless steel plates in the two positions lies between 2.77 and 2.98. Therefore, the effect of the boron plates containing more than 8 g of boron can be roughly approximated by using the above ratios. The effects of shading and enhancement were approximated for this estimate. By this method the total effectiveness for eight plates inserted in pairs in four elements in an aluminum core, each plate containing 50 g of boron, was estimated to be 12 to 14%. The effectiveness in a stainless steel core would be expected to be about one-half of the above value, since the absorption section for the stainless steel core is about double that of the aluminum core. A control this large would be satisfactory for the stainless steel reactor.

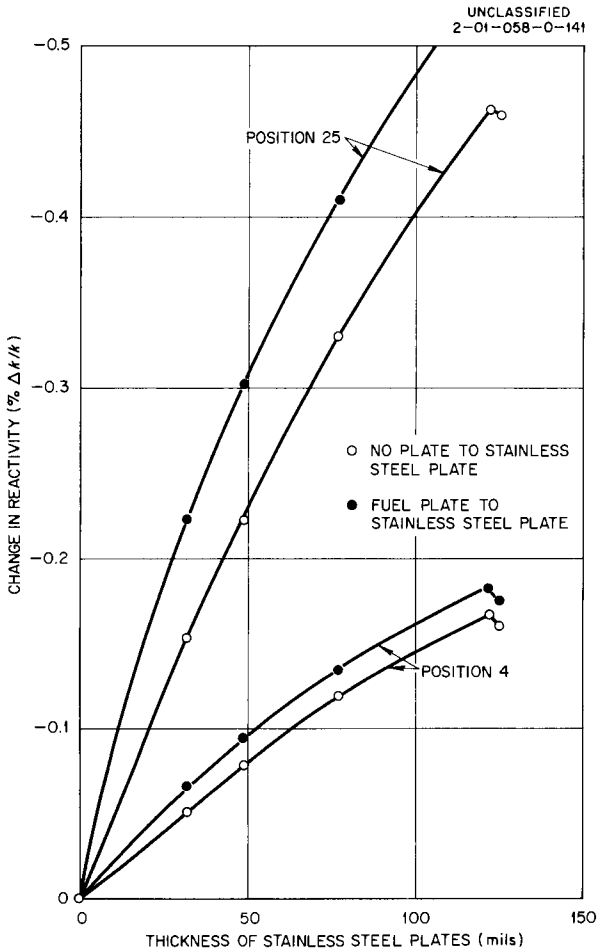

Fig. 6.3.20. Change in Reactivity Caused by Insertion of Stainless Steel Plates in Element B-151 (BSR Loading No. 57).

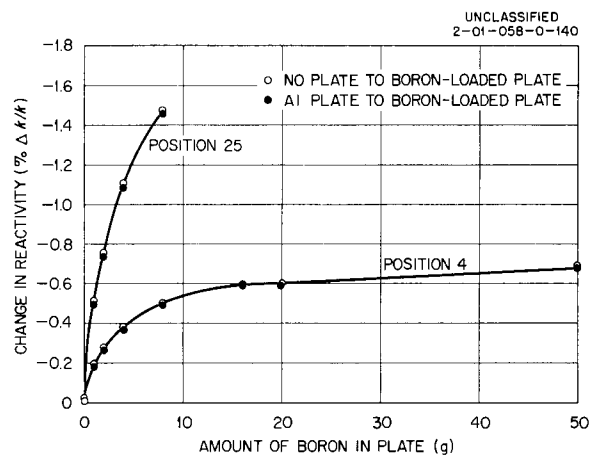

Fig. 6.3.21. Change in Reactivity Caused by Insertion of Boron-Loaded Aluminum Plates in Element B-151 (BSR Loading No. 57).